

**NASA TECHNICAL NOTE**



**NASA TN D-8013**

**NASA TN D-8013**

**CASE FILE  
COPY**

**ANALYTICAL MODELING REQUIREMENTS FOR  
TILTING PROPROPOTOR AIRCRAFT DYNAMICS**

*Wayne Johnson*

*Ames Research Center*

*and U.S. Army Air Mobility R&D Laboratory*

*Moffett Field, Calif. 94035*



**NATIONAL AERONAUTICS AND SPACE ADMINISTRATION • WASHINGTON, D. C. • JULY 1975**

1. Report No. NASA TN D-8013	2. Government Accession No.	3. Recipient's Catalog No.	
4. Title and Subtitle  ANALYTICAL MODELING REQUIREMENTS FOR TILTING PROPROTOR AIRCRAFT DYNAMICS		5. Report Date JULY 1975	6. Performing Organization Code
		8. Performing Organization Report No. A-5698	10. Work Unit No. 505-10-22
7. Author(s)  Wayne Johnson	9. Performing Organization Name and Address Ames Research Center and U.S. Army Air Mobility R&D Laboratory Moffett Field, California 94035		
12. Sponsoring Agency Name and Address National Aeronautics and Space Administration Washington, D.C. 20546		11. Contract or Grant No.	13. Type of Report and Period Covered Technical Note
		14. Sponsoring Agency Code	
15. Supplementary Notes			
16. Abstract  A theory for proprotor and cantilever wing aeroelastic behavior is applied to a gimbaled rotor and a hingeless rotor in an investigation of the requirements of an analytical model for the accurate prediction of tilting proprotor aircraft dynamics. Particular attention is given to: the influence of coupled flap/lag bending modes; the influence of rotor blade torsion degrees of freedom on proprotor dynamics; and to a constant coefficient approximation representing the dynamics in nonaxial flow through the rotor (operation in helicopter forward flight or conversion mode flight, which is properly represented by a system of periodic coefficient differential equations). Among the other factors examined are: the number of blade bending and torsion modes required, the influence of the rotor aerodynamic model, the influence of the blade trim bending deflection, the importance of the rotor rotational speed degree of freedom, and the effect of the wing aerodynamic forces. The origin of the significant influence of the blade pitch motion on the proprotor dynamics is also discussed.			
17. Key Words (Suggested by Author(s))  Rotor dynamics Tilting proprotor aircraft		18. Distribution Statement  Unclassified - Unlimited  STAR Category 39	
19. Security Classif. (of this report) Unclassified	20. Security Classif. (of this page) Unclassified	21. No. of Pages 59	22. Price* \$4.25

## NOTATION

$a$	blade section two-dimensional lift-curve slope
$C_Q$	rotor torque coefficient, $\frac{Q}{\rho(\Omega R)^2 \pi R^3}$
$C_T$	rotor thrust coefficient, $\frac{T}{\rho(\Omega R)^2 \pi R^2}$
$c$	rotor blade chord
$c_d$	blade section drag coefficient
$c_l$	blade section lift coefficient
$c_{l\alpha}$	rotor blade lift-curve slope
$I_b$	rotor flap moment of inertia
$I_p$	rotor blade pitch moment of inertia
$K_{P\zeta}$	effective pitch/lag coupling of blade, positive for lag back/pitch down
$L$	blade section lift
$m$	blade section mass per unit length
$p$	wing torsion degree of freedom
$Q$	rotor torque
$q_1$	wing vertical bending degree of freedom
$q_2$	wing chordwise bending degree of freedom
$R$	rotor radius
$r$	blade radial station
$r_{FA}$	radial location of pitch bearing
$T$	rotor thrust
$V$	forward velocity
$x$	inplane deflection of blade bending mode shape

$z$	out-of-plane deflection of blade bending mode shape
$\alpha$	blade section angle of attack
$\alpha_p$	pylon/shaft angle of attack; zero for proprotor operated in airplane cruise mode
$\beta$	notation for rotor coning mode
$\beta - 1$	notation for rotor low frequency flap mode
$\beta + 1$	notation for rotor high frequency flap mode
$\beta_0$	rotor coning degree of freedom
$\beta_{1c}$	rotor-tip-path plane pitch degree of freedom
$\beta_{1s}$	rotor-tip-path-plane yaw degree of freedom
$\beta_p$	blade precone angle
$\beta_{trim}$	trim elastic coning deflection of blade
$\gamma$	blade Lock number, $\gamma = \frac{\rho a c R^4}{I_b}$
$\delta_3$	pitch/flap coupling
$\zeta$	damping ratio of eigenvalue, fraction of critical damping
$\zeta - 1$	notation for rotor low-frequency lag mode
$\zeta + 1$	notation for rotor high-frequency lag mode
$\zeta_0$	rotor collective lag degree of freedom
$\zeta_{1c}$	cyclic lag degree of freedom (rotor lateral CG shift)
$\zeta_{1s}$	cyclic lag degree of freedom (rotor vertical CG shift)
$\eta$	blade bending mode shape (function of $r$ )
$\eta'(r_{FA})$	slope of bending mode at pitch bearing
$\theta$	blade torsion mode shape
$\theta_{.75}$	rotor collective pitch angle, at 75 percent radius

$\lambda$	eigenvalue or root of system
$\lambda$	inflow ratio: component of aircraft velocity normal to rotor plane, divided by the rotor tip speed
$\mu$	advance ratio: component of aircraft velocity in plane of rotor disk, divided by the rotor tip speed
$\nu$	rotating natural frequency of blade bending mode
$\nu_\beta$	rotating natural frequency of blade flap mode
$\nu_\xi$	rotating natural frequency of blade lag mode
$\rho$	air density
$\sigma$	rotor solidity ratio
$\psi_s$	rotational speed perturbation degree of freedom
$\omega$	nonrotating natural frequency of blade torsion mode
$\omega_\theta$	natural frequency of blade rigid pitch motion (control system stiffness)
$\Omega$	rotor rotational speed

# ANALYTICAL MODELING REQUIREMENTS FOR TILTING PROPROTOR AIRCRAFT DYNAMICS

Wayne Johnson

Ames Research Center  
and  
U.S. Army Air Mobility R&D Laboratory

## SUMMARY

A theory for proprotor and cantilever wing aeroelastic behavior is applied to a gimbaled rotor and a hingeless rotor in an investigation of the requirements of an analytical model for the accurate prediction of tilting proprotor aircraft dynamics. Particular attention is given to: the influence of coupled flap/lag bending modes; the influence of rotor blade torsion degrees of freedom on proprotor dynamics; and to a constant coefficient approximation representing the dynamics in nonaxial flow through the rotor (operation in helicopter forward flight or conversion mode flight, which is properly represented by a system of periodic coefficient differential equations). Among the other factors examined are: the number of blade bending and torsion modes required, the influence of the rotor aerodynamic model, the influence of the blade trim bending deflection, the importance of the rotor rotational speed degree of freedom, and the effect of the wing aerodynamic forces. The origin of the significant influence of the blade pitch motion on the proprotor dynamics is also discussed.

## INTRODUCTION

The tilting proprotor aircraft is a promising concept for short-haul, V/STOL missions. This aircraft uses low disk-loading rotors located on the wing tips to provide lift and control in hover and low-speed flight; the same rotors are used to provide propulsive force in high-speed cruise with the lift supplied by a conventional wing. Such operation requires a  $90^\circ$  change in the rotor thrust direction by mechanically tilting the rotor shaft axis. Thus the aircraft combines the efficient VTOL capability of the helicopter with the efficient high-speed cruise capability of a turboprop aircraft. The combination of low disk-loading, flapping rotors, operating in cruise mode at a high inflow ratio (the ratio of axial velocity to rotor tip speed) and located on the tips of flexible wings, leads to dynamic and aeroelastic characteristics that are in many ways unique to this configuration. In order to take full advantage of the efficient VTOL and high-speed cruise capabilities, it is important to establish a clear understanding of the dynamic characteristics of this aircraft and to determine adequate methods of predicting them. A number of experimental and theoretical investigations directed at providing this capability have been conducted (see, e.g., the discussion in ref. 1). It remains, however, to establish exactly what constitutes a sufficient analytical model for the accurate prediction of tilting proprotor aircraft dynamics. This paper presents the results of a theoretical investigation of that question.

An analytical model for tilting proprotor aircraft dynamics was developed previously by the author in reference 2. The model for the rotor includes coupled flap/lag bending modes and the

blade torsion degrees of freedom. The rotor aerodynamic model is generally valid for high and low inflow, and for axial and nonaxial flight. The emphasis in reference 2 is on the development of the rotor theory, with a cantilever wing model to represent the proprotor support dynamics. Figure 1 shows a full-scale rotor in the Ames 40- by 80-Foot Wind Tunnel, illustrating the configuration of the proprotor operating at high inflow on a cantilever wing. Such a support is sufficient for both theoretical and experimental investigations of the rotor dynamics and of the general aeroelastic characteristics of tilting proprotor aircraft. Prediction of the dynamic stability level of a specific aircraft would of course require a theoretical model extended to the complete vehicle, coupled with the rotor model of reference 2.

In this report we shall examine the behavior predicted for the rotor and cantilever wing configuration, with the intention of establishing what is required of a mathematical model to satisfactorily represent the dynamics. To conduct this investigation, the theory is applied to two full-scale proprotor designs: a gimballed, stiff-inplane rotor and a hingeless, soft-inplane rotor. The elements of the analytical model to be examined include the number of degrees of freedom for the rotor blade bending and torsion motion, nonaxial flow through the rotor, and various approximations in the rotor structural and aerodynamic model. We begin with a discussion of the basic features of the analytical model.

## ANALYTICAL MODEL

The analytical model for the proprotor and cantilever wing dynamic system is derived in reference 2. The equations of motion for the rotor degrees of freedom are developed, including inputs from shaft motion, rotor collective and cyclic pitch control, and aerodynamic gust components; expressions for the hub forces and moments are also obtained. The equations for the cantilever wing support, excited by the rotor hub forces and moments, are presented, including inputs from a wing flaperon control and aerodynamic gusts. The shaft motion produced by the wing degrees of freedom is also derived. The rotor and wing equations are then combined to give the equations of motion for the complete proprotor and cantilever wing system.

The following paragraphs describe the analytical model for the rotor and wing. First, there is a discussion of the geometry and motion of the system, including the basic assumptions of the theory. This discussion concludes with a summary of the rotor motion. Next, the modal representation of the motion, which transforms the bending and torsion motion of the blades into the degrees of freedom for the dynamic analysis, is described. The remaining paragraphs in this section deal with several specific elements of the analytical model. The next section then presents a summary of the degrees of freedom used to represent the proprotor and wing dynamics.

### Geometry and Motion

The rotor model consists of coupled flap/lag bending of the blades, rigid pitch deflection (due to control system flexibility), blade elastic torsion deflection, gimbal tilt (pitch and yaw), and a rotor rotational speed perturbation degree of freedom. The gimbal and rotor speed degrees of freedom are optional. It is assumed that the blades have a high aspect ratio, so engineering beam theory and lifting line theory are applicable. When the flow is axial, the model is valid for rotors

with three or more blades; for nonaxial flow (the periodic coefficient case) it is restricted to three-bladed rotors. Blade precone and pitch bearing radial offset (the latter for the case of a rotor with bending flexibility inboard of the pitch bearing) as well as offsets of the blade section center of gravity and aerodynamic center from the elastic axis, are included. The elastic axis is assumed to be a straight line coincident with the feathering axis. The model also includes the effects of large pitch and twist of the blade in the structural, inertial, and aerodynamic models; effects of the trim bending deflection of the blade (the mean value for nonaxial flow); and the effects of the trim distribution of aerodynamic forces over the rotor disk. The rotor is assumed to be operating in a steady free stream of velocity  $V$ , at an arbitrary shaft angle of attack  $\alpha_p$ . The rotor aerodynamic model is generally valid for high and low inflow, and for axial and nonaxial flight. The effects of compressible flow and static stall are included in the blade section aerodynamic characteristics. Uniform rotor induced inflow is assumed, and unsteady wake aerodynamic interference effects of the rotor are neglected. The effects of the wing wake on the rotor and all other wing/rotor aerodynamic interferences are neglected.

A cantilever wing support was used in this investigation (fig. 1). The proprotor and cantilever wing configuration incorporates the features of greatest importance to the tilting proprotor aircraft dynamics, namely the high inflow aerodynamics of a flapping rotor, and the coupled dynamics of the rotor and wing aeroelastic system. Hence this configuration is suitable for the present study of the analytical model that is required for an adequate representation of the dynamics, with emphasis on the rotor elements. Moreover, full-scale and model test results are available for the cantilever wing and proprotor configuration. An investigation of the dynamic behavior of an actual proprotor aircraft would of course require the replacement of the cantilever wing by a more complete support model.

For the present work, the support model assumed is a high aspect-ratio, flexible wing with a pylon and rotor shaft attached rigidly to the tip; the wing root is attached to an immovable support with cantilever restraint. The wing motion consists of elastic bending (vertical and chordwise) and elastic torsion. A modal representation of the wing bending and torsion motion is used, and the three degrees of freedom corresponding to the lowest frequency modes – wing vertical bending ( $q_1$ ), wing chordwise bending ( $q_2$ ), and wing torsion ( $p$ ) – are retained. There is no motion of the pylon with respect to the wing tip, hence there is direct transmission of the wing tip motion to the rotor, and of the hub forces and moments to the wing. The wing and rotor operate in a steady free stream at velocity  $V$ . Wing aerodynamic forces are included, based on a strip-theory calculation of the coefficients. An arbitrary angle of attack ( $\alpha_p$ ) of the rotor shaft with respect to the free-stream velocity is considered. It ranges from vertical in the helicopter mode to horizontal in the airplane mode, hence covering the entire range of tilting proprotor aircraft operation. That is, the angle  $\alpha_p$  is near  $90^\circ$  for the helicopter mode, between  $0^\circ$  and  $90^\circ$  for the conversion mode, and zero for the cruise mode.

In summary, the rotor motion is described by the following model, beginning at the shaft. First there is the shaft motion due to the support degrees of freedom. Next there is the rotor rotational speed degree of freedom, and two degrees of freedom for tilt of the hub (gimbal pitch and yaw). At this point the hub precone is entered, defining the orientation of the blade root with respect to the hub. Next there is bending of the blade elastic axis with respect to the hub, with cantilever root restraint. The pitch bearing is located at radial station  $r_{FA}$ . If  $r_{FA} > 0$ , there is bending flexibility inboard of the pitch bearing, and hence a slope and displacement change of the feathering axis occurs due to bending. There is rigid pitch motion of the blade about the feathering

axis due to control system flexibility. Finally, there is elastic torsion motion of the blade with no motion about the pitch axis at the root. For a hingeless rotor, the degrees of freedom and equations corresponding to the gimbal motion are dropped.

### Blade Modes

A modal representation is used for the blade bending and elastic torsion motion. The bending and torsion deflection are expanded as infinite series in the free vibration modes of the blade. This expansion separates the spatial variation of the motion (which is accounted for by the mode shapes) and the time variation (which is in the modal degrees of freedom). One of the questions to be examined here is how many of the bending and torsion modes – hence how many rotor degrees of freedom – are required for a sufficient representation of the prop rotor dynamics.

For the bending motion, the free vibration modes of coupled flap/lag bending of a rotating blade are used (including therefore the centrifugal stiffening). For the rotors examined here, cantilever root boundary conditions are used for the individual blade bending modes. For the torsion motion, the free vibration modes of elastic torsion of a nonrotating blade are used, with no pitch displacement at the root. The bending modes are first made dimensionless by dividing by the rotor radius  $R$ , and then normalized to unit amplitude at the tip. The torsion modes give the pitch displacement in radians, and are normalized to unity at the blade tip. Calculation of the mode shapes is described in reference 2.

Another objective of this work is to examine the effect of the coupled flap/lag bending of the blades on the prop rotor and wing dynamics. Gimballed and hingeless rotor designs typically exhibit significant coupling of the flap and lag motion; that is, there is participation of both out-of-plane and inplane motion in each bending mode. A comparison is made of calculations using coupled and uncoupled bending modes. For the case with uncoupled modes, the flap mode is pure out-of-plane motion, and the lag mode is pure inplane motion. A mode shape of  $\eta = r/R$  is used for the uncoupled case, corresponding to rigid body rotation about a flap or lag hinge at the rotor center of rotation. (The effects which will be seen for the uncoupled case are primarily due to the elimination of the coupling rather than the change in the mode shape; this is because the high centrifugal forces cause the blade fundamental modes to always have a shape similar to  $\eta = r/R$ .) The same bending mode natural frequencies are used for both the coupled and uncoupled mode calculations.

### Treatment of Torsion

For the treatment of the rotor pitch and torsion motion, three options are considered. First there is the no-torsion case which is the limit of infinite control-system and blade-torsion stiffness. In this case the rotor blade elastic torsion motion is zero, and the rigid pitch motion is not a degree of freedom but just an input to the other equations, consisting of blade pitch control and kinematic feedback of the blade bending and gimbal motion (pitch/flap and pitch/lag coupling inherent in the hub and root geometry). In the second option, the pitch and torsion modes are included as degrees of freedom in the dynamic system.

The third option is a quasi-static torsion approximation, in which the acceleration and velocity terms due to the torsion and pitch degrees of freedom are neglected. The torsion equations then

become just static substitution relations for the blade pitch in the other equations of motion. This treatment retains all of the static coupling effects in the torsion equations of motion, not just the kinematic pitch/bending and pitch/gimbal coupling as in the no-torsion case. For a further description of these three options, including the details of their implementation, see reference 2.

### Rotational Speed Degree of Freedom

The rotor speed perturbation degree of freedom ( $\dot{\psi}_s$ ) has an important influence on the aeroelastic behavior of the proprotor and wing system. This degree of freedom usually involves the dynamics of the engine, drive train, and governor, but here only two limiting cases are considered. In the first case, the rotor is operated unpowered, that is, windmilling or autorotation operation. The rotor is free to turn on the shaft, and the equation of motion for this degree of freedom is given by simply  $C_Q = 0$ . In the second case, the rotor hub angular velocity is assumed to be constant, with no perturbation. The rotor azimuth and rotational speed are measured with respect to the pylon, hence pylon roll motion is transmitted to the rotor. Also, shaft torque moments from the rotor are transmitted to the pylon and wing tip. The solution for this case is  $\psi_s \equiv 0$ , so the rotor speed perturbation degree of freedom and equation are dropped from the system. This case is taken to represent powered operation of the rotor, although it is really the limit of operation with a perfect governor on rotor or engine speed.

The results presented here are mainly for the case of a windmilling rotor. This case is probably a good model for general proprotor and wing dynamics because the dynamics of the engine, drive train and governor will have a long time-constant compared to the rotor and wing modes. Hence for the frequency range characteristic of this system, the rotor should behave as if windmilling even though the engine and governor are operating. This assumption is undoubtedly not always true, but it is a good simplification for the present purposes. In addition, there are dynamic test data available for the windmilling rotor.

### Rotor Aerodynamic Model

The basic aerodynamics of the proprotor operating in high inflow axial flight are simpler than those of the low-inflow rotor in forward flight (the helicopter). The symmetry of axial flow results in a corresponding symmetry in the equations of motion, and means that the differential equations of motion have constant coefficients (as for the case of low-inflow axial flight, i.e., the hovering helicopter rotor). In the high-inflow case there is an additional factor: both out-of-plane and inplane motion of the blade produce a significant angle-of-attack change at the blade section, and the resulting lift increment has significant components both normal to and in the disk plane. The primary contribution to the rotor aerodynamic forces is due to these lift changes produced by angle-of-attack changes of the blade section. Hence the  $c_{l\alpha}$  terms dominate the aerodynamic coefficients of the rotor. This is in contrast to low inflow where, for example, inplane blade motion produces significant contributions to the forces because of the lift and drag increments that result from the dynamic pressure changes, and because of the tilt of the trim lift and drag – that is, the  $c_l$  and  $c_d$  terms in the aerodynamic coefficients. If just the  $c_{l\alpha}$  forces are considered, the rotor aerodynamic coefficients depend on only two parameters: the Lock number  $\gamma$ , and the inflow ratio  $V/\Omega R$ . These are, therefore, the dominant aerodynamic parameters determining the proprotor aeroelastic behavior. For a further discussion of the high inflow rotor aerodynamic coefficients, see reference 1.

The complete rotor aerodynamic model (the  $c_{l\alpha}$ ,  $c_l$ ,  $c_d$ , and  $c_{d\alpha}$  terms, and the derivatives with respect to Mach number are retained in the aerodynamic coefficients) will be taken as the standard case in the applications of the theory presented here. How much of the dynamic behavior is determined by the  $c_{l\alpha}$  rotor forces will be examined by comparing calculations using the complete aerodynamic model, and using only the  $c_{l\alpha}$  terms.

### Nonaxial Flow

One of the primary objectives of the present work is to examine the influence of the periodic coefficients on the dynamics, and especially the applicability of a constant coefficient approximation to the nonaxial flow operation of the tilting proprotor aircraft. The analytical model for the proprotor and wing includes an arbitrary angle of attack of the pylon and rotor shaft ( $\alpha_p$ ). The differential equations are derived in reference 2 for the following three cases. The first case is axial flow ( $\mu = 0$ ;  $\lambda$  small for hover and order 1 for cruise), which is a constant coefficient system. The second case is nonaxial flow ( $\mu > 0$ ;  $\lambda$  small for helicopter forward flight and order 1 for conversion mode flight), which is properly a periodic coefficient system due to the periodically varying aerodynamics of the edgewise-moving rotor. The third case is a constant coefficient approximation for the nonaxial flow equations, using the mean values of the coefficients (in the nonrotating frame). A constant coefficient approximation is desirable (if it is demonstrated to be accurate enough) because the calculation required for the system analysis is considerably reduced compared to the periodic coefficient equations, and because the powerful techniques for analyzing time-invariant (constant coefficient) linear differential equations are applicable. It is only an approximation to the correct dynamics, however. The accuracy of the approximation must be determined by comparison with the correct periodic coefficient solutions. The axial flow case is applicable to the proprotor aircraft in airplane-mode cruise and in helicopter-mode hover flight. The nonaxial flow case is applicable to helicopter forward flight and to conversion-mode flight of the proprotor aircraft.

### DEGREES OF FREEDOM AND STANDARD CASE

Summarizing the preceding description, the analytical model for the rotor and cantilever wing consists of the following degrees of freedom: an arbitrary number of coupled flap/lag bending modes per blade; a rigid-pitch mode and an arbitrary number of elastic torsion modes per blade; and vertical bending, chordwise bending, and torsion for the cantilever wing. The gimbal and rotor speed perturbation degrees of freedom are also included as appropriate. The following model is adopted as a standard case for the examination of the proprotor analytical model:

1. Two coupled bending modes per blade (fundamental flap and lag modes).
2. No blade pitch or torsion degrees of freedom.
3. All three wing degrees of freedom.
4. Complete rotor aerodynamic model.
5. Wing aerodynamics included.

6. Windmilling rotor.

7. Operation in airplane cruise mode ( $\alpha_p = 0$ , high-inflow axial flight).

The basic model thus consists of nine degrees of freedom: vertical bending, chordwise bending, and torsion for the wing; and for each of the three blades, the two lowest frequency bending modes (one of which is predominantly out-of-plane motion, and one predominantly inplane motion). For a gimballed rotor the two gimbal degrees of freedom replace the cyclic out-of-plane bending degrees of freedom in the basic model.

The degrees of freedom of the individual rotor blades are combined into degrees of freedom representing the motion of the rotor as a whole in the nonrotating frame. Thus the rotor flap motion is represented by the tip-path plane pitch and yaw ( $\beta_{1c}$  and  $\beta_{1s}$ ) and coning ( $\beta_0$ ) degrees of freedom; the rotor lag motion is represented by cyclic lag degrees of freedom,  $\zeta_{1c}$  and  $\zeta_{1s}$  (which produce respectively lateral and vertical shifts of the rotor net center of gravity) and by the collective lag degree of freedom,  $\zeta_0$ . (For helicopter rather than proprotor orientation of the rotor,  $\beta_{1c}$  and  $\beta_{1s}$  are tip-path plane pitch and roll, while  $\zeta_{1c}$  and  $\zeta_{1s}$  produce lateral and longitudinal shifts of the rotor center of gravity.) Wing vertical and chordwise bending ( $q_1$  and  $q_2$ ) and torsion ( $p$ ) complete the basic set of degrees of freedom.

This nine-degree-of-freedom model will have nine roots or eigenvalues (really nine pairs of complex roots) and correspondingly nine eigenvectors or modes. Of course, each mode involves motion of all nine degrees of freedom. The modes are identifiable by their frequencies (which will be near the uncoupled natural frequencies of the system, in the nonrotating frame for the rotor modes) and also by the participation of the nine degrees of freedom in the eigenvectors. The nine modes will be denoted as follows (the approximate, uncoupled natural frequency of the mode is given in parentheses):

$\beta$	coning ( $\nu_\beta$ )
$\beta - 1$	low-frequency flap ( $\nu_\beta - \Omega$ )
$\beta + 1$	high-frequency flap ( $\nu_\beta + \Omega$ )
$\zeta$	collective lag ( $\nu_\zeta$ )
$\zeta - 1$	low-frequency lag ( $\nu_\zeta - \Omega$ )
$\zeta + 1$	high-frequency lag ( $\nu_\zeta + \Omega$ )
$q_1$	wing vertical bending ( $\omega_{q_1}$ )
$q_2$	wing chordwise bending ( $\omega_{q_2}$ )
$p$	wing torsion ( $\omega_p$ )

For the windmilling rotor the rotational speed degree of freedom replaces the collective lag as a fundamental mode. This mode is then a well-damped convergence (negative real root) since there is no spring force on the rotor azimuth perturbation. For the gimbaled rotor the  $\beta \pm 1$  modes are gimbal tilt, while the coning mode involves elastic out-of-plane bending of the blade. Because it is a cantilever mode, the coning motion has a much higher natural frequency than the gimbal motion.

The blade rigid-pitch motion is the fundamental mode when the pitch degrees of freedom of the blade are included. The control system is usually the softest element in the torsion motion, so the rigid-pitch mode has the lowest frequency (although it is still usually much higher than the rotor bending and wing frequencies). The degrees of freedom in the nonrotating frame are collective and cyclic pitch. They add to the system a collective mode and low and high frequency cyclic modes, with corresponding natural frequencies  $\omega_\theta$  and  $\omega_\theta \pm \Omega$ . As higher bending modes, torsion modes, and support modes are added to the system, they take their place in a structure similar to that of the basic model described above.

## TWO FULL-SCALE PROPROTORS

Two full-scale proprotors are considered for application of the theory: a gimbaled, stiff-inplane rotor and a hingeless, soft-inplane rotor. Full-scale design data and results from tests in the NASA Ames 40- by 80-Foot Wind Tunnel are available for these rotors (ref. 1). The full-scale tests were conducted with the windmilling rotor on a cantilever wing (fig. 1) which had properties similar to the wing of a representative full-scale aircraft design. The properties of this cantilever wing were used for the calculations presented here.

As far as their dynamic characteristics are concerned, the two rotors differ primarily in the placement of the rotating natural frequencies of the fundamental blade flap and lag modes. The gimbaled, stiff-inplane rotor has a flap frequency slightly above 1/rev (due to a hub spring), and a lag frequency above 1/rev. It also incorporates positive pitch/flap coupling ( $\delta_3 < 0$ ), so that the negative aerodynamic spring reduces the effective flap frequency somewhat below 1/rev (for increased blade flap/lag stability). The hingeless, soft-inplane rotor has a flap frequency above 1/rev and a lag frequency below 1/rev. The different placement of the fundamental blade frequencies results in quite different dynamic characteristics for the two aircraft.

A description of the rotors and the cantilever wing is given in appendix A. Table I presents the major parameters of the rotor and cantilever wing used for the theoretical results in this work. The bending and torsion mode shapes and frequencies are presented in the discussion of the results to follow. Both rotors have  $2.5^\circ$  of precone. The gimbaled rotor has a pitch bearing radial location of  $0.09R$  with bending flexibility inboard of the feathering axis. The hingeless rotor has the pitch bearing located in the rigid hub, so there is essentially no movement of the feathering axis with bending of the blade. The rotor Lock number is based on sea level density.

## OUTLINE OF INVESTIGATION

To establish the analytical modeling requirements for a tilting proprotor aircraft, the dynamic stability of the proprotor and cantilever wing system (the frequency and damping ratio of the

modes) will be examined. Particular attention is given to the damping ratio of the three wing modes. These are the critical roots of the system, characterized by the lowest damping level and usually by an instability at high speed. The basic dynamic stability will be examined in terms of a root locus and the variation of the damping ratios with speed; the predictions will be compared with some full-scale test data. The analytical model will then be examined by considering the following cases, comparing each with the standard case:

1. Influence of the blade lag motion, by dropping the cyclic lag degrees of freedom ( $\xi_{1c}$  and  $\xi_{1s}$ ).
2. Wing aerodynamics influence, by omitting the wing aerodynamic forces.
3. Rotor speed perturbation influence, by considering the powered case (dropping  $\dot{\psi}_s$  and reinstating the collective lag degree of freedom).
4. The effect of using only the  $c_{l\alpha}$  terms in the rotor aerodynamic coefficients.
5. The effect of using uncoupled blade modes.
6. The effect of including higher blade bending modes.
7. Influence of the blade torsion/pitch degrees of freedom on the dynamics.
8. Influence of the blade trim bending deflection, by setting it to zero.
9. Accuracy of the constant coefficient approximation to the dynamics in nonaxial flow ( $\mu > 0$ ), by comparing it with the correct periodic coefficient solution.

Cases 1 through 4 duplicate to some extent the results in reference 1, which were obtained using a simpler analytical model. Hence the results of cases 1 through 4 also provide further verification of the present theory.

## RESULTS AND DISCUSSION: GIMBALLED ROTOR

In this section the dynamic stability of the gimbaled rotor is examined. We begin with a presentation of the blade bending and torsion modes, which were calculated by the methods described in reference 2 from the blade mass and stiffness distributions given in appendix A. The bending modes were calculated for the windmilling rotor, but the collective pitch change from windmilling to powered operation is so small that these results represent the powered case as well.

Figure 2 shows the natural frequencies of the bending modes of the gimbaled rotor, as a function of forward speed for cruise-mode rotor speed ( $\Omega = 458$  rpm). These are the cantilever bending modes of a single blade. The variation with speed is due to the collective pitch change with inflow ratio. The gimbal mode frequency is also shown. Figure 3 shows the tip deflection of the first three bending modes. In figure 3, the rotor hub plane is vertical (proprotor orientation) and the shaft axis and forward velocity are horizontal. The first mode is predominantly inplane motion, and

the second predominantly out-of-plane motion, but there is substantial flap/lag coupling of the modes, especially at the lower speeds. For reference, the orientation of the blade root section is also shown; the first and second modes are primarily beamwise and chordwise bending about the root section. Figure 4 shows typical bending mode shapes, at  $V/\Omega R = 0.7$ : the radial variation of the inplane ( $x$ ) and out-of-plane ( $z$ ) components of the bending deflection. There is substantial flap/lag coupling evident in each mode. Figure 5 shows the mode shapes and frequencies for the blade uncoupled rigid pitch and elastic torsion motion. The first mode is rigid pitch of the blade, due to control system flexibility, with a natural frequency of 4.8/rev. The higher modes are elastic torsion of the blade with no motion at the pitch bearing. The frequencies given are per-rev values at  $\Omega = 458$  rpm; however, the mode shapes and dimensional frequencies are really independent of the rotor collective pitch and rotational speed, because nonrotating torsion modes are used. The rigid pitch and first elastic torsion modes combine in the dynamics to give a coupled mode which is composed of about 50 percent rigid and 50 percent elastic motion, with a natural frequency of 4.3/rev.

Figure 6 gives the trim deflection of the first two bending modes for windmilling ( $C_Q = 0$ ) and powered (cruise  $C_T$ ) operation of the rotor in airplane cruise mode. There is negative elastic coning of the rotor in both powered and windmilling operation, because of the low loading of the rotor in cruise flight. The rotor precone of  $2.5^\circ$ , was chosen for the high loading of hover, and hence is too high for cruise. The elastic coning is small, however, due to the high coning stiffness of the gimballed rotor. The large trim lag deflection of the powered rotor at high speed reflects the power increase to achieve the rotor thrust required.

#### Standard Case

The basic dynamics of the gimballed rotor and wing are shown in figure 7 which is a root locus for a velocity sweep from 100 to 500 knots. The case presented is that of a windmilling rotor with no torsion. The eight primary modes discussed above are shown. The rotational speed mode is not shown, as it is a well damped convergence, that is, a root on the negative real axis. Figure 8 presents the variation with speed of the damping ratio of the three wing modes: wing vertical bending ( $q_1$ ), chordwise bending ( $q_2$ ), and wing torsion ( $p$ ). All three modes become unstable at high speed, the critical mode for this case being the vertical bending mode, giving a stability boundary at  $V = 450$  knots. The predicted wing vertical bending mode damping is compared with the results of a full-scale test of this rotor and cantilever wing in the NASA-Ames 40- by 80-Foot Wind Tunnel (ref. 1), and good correlation is shown.

#### Elements of the Analytical Model

Figure 9 shows the influence of the rotor lag motion on the damping of the wing modes, by comparing the predicted stability with and without the cyclic lag degrees of freedom (the first bending mode). The rotor low-frequency lag mode ( $\zeta - 1$ ) has an important influence on the dynamics, particularly on the wing vertical bending mode ( $q_1$ ). The increase in the  $q_1$  damping below 250 knots, compared to the no lag-motion case, is due to a resonance of the  $\zeta - 1$  and  $q_1$  mode frequencies. These results agree with those of reference 1, where a more extensive discussion of the role of the rotor lag degrees of freedom is given. Figure 10 shows the influence of constant rotor speed operation (stabilizing) and of omitting the wing aerodynamics (destabilizing). With the

rotor speed fixed (with respect to the pylon), the pylon roll due to the wing vertical bending motion produces a roll motion of the rotor. The high aerodynamic damping of this rotor motion (similar to the blade lag damping, which is large for high-inflow operation) is the source of the general increase in the system stability when the rotor speed perturbation is dropped. The wing aerodynamics contribute significantly to the stability, especially that of the  $q_1$  mode; the effect is mainly caused by aerodynamic damping of the wing modes that results from changes in the angle of attack during the motion. The influence of the trim bending deflection was examined by setting it to zero in the calculations; only negligible effect was found (for this case with no blade-torsion degrees of freedom), and the results are not plotted.

Figure 11 shows the effects of using uncoupled blade bending modes, and of using only the  $c_{l\alpha}$  terms in the rotor aerodynamics. The effect of the coupled flap/lag bending modes is quite substantial. Using uncoupled modes results in a sharper damping increase for the wing vertical bending mode at the  $\zeta - 1$  and  $q_1$  resonance (around 160 knots), and a significant change in the instability speed. It should be noted that for this gimbaled, windmilling rotor the only modes involving coupled inplane/out-of-plane motion are the cyclic lag ( $\zeta \pm 1$ ) and coning modes, and it is the former that contributes almost all of the effects shown in figure 11. Comparing figures 9 and 11, it is found that virtually the same stability boundary is obtained using uncoupled modes as for the case without the lag motion. It follows therefore that the change in the high speed stability boundary in figure 9 is due to the out-of-plane motion in the lag mode. Using only the  $c_{l\alpha}$  terms in the rotor aerodynamics produces a general increase in the wing mode damping at high speed, and a corresponding increase in the speeds for instability of the modes. The form of the curves remains the same, however, and there is no change in the basic character of the dynamics. It is concluded that the basic dynamic behavior is determined by the  $c_{l\alpha}$  rotor aerodynamic forces; however, at very high speed the  $c_l$ ,  $c_d$ , and other terms in the aerodynamic coefficients, become important even at high inflow. Figure 12 shows the effect of using both uncoupled bending modes and only the  $c_{l\alpha}$  terms in the rotor aerodynamics. This recovers the standard case of reference 1, and the results of the present theory and of that earlier analysis compare well. The effects in figure 12 are a direct combination of what was shown in figure 11 for the separate cases of uncoupled modes and only  $c_{l\alpha}$  rotor aerodynamics.

Figure 13 shows the effect of using two or three bending modes per blade, compared with the standard case. Using two bending modes per blade (plus the gimbal and rotor speed degrees of freedom), results in a nine-degree-of-freedom model for the proprotor, compared to six rotor degrees of freedom for the standard case. The three added degrees of freedom are the collective lag from the first bending mode, and the cyclic flap from the second mode. The rotor motion produced by these degrees of freedom is similar to that produced by the rotational speed perturbation and gimbal tilt degrees of freedom. Hence the primary effect of the added degrees of freedom is to improve the representation of the rotor motion already in the basic model. The additional eigenvalues and eigenvectors corresponding directly to the three new degrees of freedom are high frequency modes and have little effect on the proprotor dynamics. Consequently, figure 13 shows that using two complete bending modes per blade improves somewhat the details of the predicted dynamics, but does not change the basic features. Using three bending modes per blade (a twelve-degree-of-freedom model for the rotor) produces little further improvement in the calculations over that obtained by using two bending modes.

## Blade Torsion

The analytical results presented so far have been for a rotor with no torsion degrees of freedom, that is, the limit of infinite control-system and blade-torsion stiffness. The influence of the blade rigid pitch and elastic torsion degrees of freedom on the proprotor and wing dynamics now will be examined. Figure 14 presents a root locus during a velocity sweep from 100 to 400 knots for a windmilling rotor, including the blade torsion dynamics. The torsion/pitch modes give high frequency roots, off the scale of figure 14. When compared with the no-torsion results (fig. 7), there is a substantial influence of the blade torsion degrees of freedom on both the wing and rotor modes. Figure 15 shows the effect of the torsion motion on the damping ratio of the wing modes. Compared to the results without torsion, there is a substantial reduction in the dynamic stability at high speed due to the blade pitch motion. There is little difference between the results using one, two, or three torsion modes. Hence the effects are primarily due to the first mode (blade rigid-pitch motion).

It is concluded that the blade pitch degree of freedom should be included in the rotor model. A satisfactory model for the proprotor is then at least nine degrees of freedom (the rigid pitch mode and two bending modes per blade). There is some improvement in the details of the basic dynamics, however, if two complete bending modes and two torsion modes per blade are used (a fifteen-degree-of-freedom-rotor model; see figs. 13 and 15). Figure 16 compares the full-scale test results for the wing vertical bending damping ratio with the predictions using several analytical models. Including the torsion dynamics improves the correlation slightly, but the difference is really within the accuracy of the experimental data. The important effects of the torsion motion are at speeds above that where the full-scale data are available.

Figure 17 examines the influence of the rotor trim bending deflections by setting it to zero in the calculations. Some effects on the wing mode stability are observed, but evidently the trim deflection is not the dominant factor in the torsion dynamics for this rotor (because the trim coning and lag deflection are small for this rotor, as shown in fig. 6). The trim deflection has considerably more influence, however, on the rotor modes and roots. In general, the blade-trim bending deflection must be included for an accurate representation of the rotor and wing dynamics when the blade torsion motion is involved. Figure 17 also shows the calculated damping using the quasi-static approximation for the torsion dynamics (dropping the acceleration and velocity terms in the pitch/torsion dynamics, as discussed above). Compared with the results using the complete torsion dynamics, essentially the same stability is obtained for the lower frequency wing modes, but not for the wing torsion mode. It is concluded that the influence of the torsion motion on the proprotor dynamics is primarily a quasi-static effect (for this rotor). In general, however, it is probably best to retain the blade torsion degrees of freedom even for this rotor, in view of the uncertain range of the validity of the quasi-static approximation.

Figure 18 compares the predicted stability using two or three bending modes per blade, with the torsion dynamics now included. There is little effect of the third bending mode even with the blade torsion motion included. Further discussion of the origin of the effects of the blade pitch degree of freedom on the proprotor and wing dynamics is given in appendix B.

## Periodic Coefficients

The proprotor dynamics will now be examined for a flight path from hover through helicopter-forward flight, conversion, and airplane-mode cruise to 300 knots. The principal objective is to investigate the effect of the periodic coefficients in helicopter-forward flight and conversion-mode flight, where  $\mu > 0$ . Figure 19 shows the variation of the operating parameters along the flight path considered. Starting from hover, helicopter mode operation extends to 80 knots. The pylon angle is converted to horizontal for  $V = 80$  to 140 knots. Then, in airplane mode,  $V = 140$  to 160 knots, the flaps are raised and the rotor speed is reduced from 565 to 458 rpm. Airplane-mode cruise then extends to 300 knots. The conversion path used corresponds roughly to the center of the conversion corridor of a representative tilting proprotor aircraft. The conversion of this aircraft from helicopter to airplane mode would be accomplished typically in about 10 sec; hence it is satisfactory to neglect the effects of acceleration along the flight path and to calculate the dynamics for operation in steady equilibrium flight at each point. A maximum advance ratio of about  $\mu = 0.2$  is encountered at the end of helicopter-forward flight and the beginning of conversion. The rotor thrust required for trim level flight is used at each point. The reduction of  $\alpha_p$  in helicopter-forward flight results from the change in body attitude as the aircraft increases speed, while the pylon angle with respect to the fuselage remains fixed at  $90^\circ$ .

Figure 20 shows the damping ratio of the three wing modes along this flight path. The analytical model used is the proprotor and cantilever wing, with a constant rotor speed (powered operation) and no blade-torsion degrees of freedom. In helicopter-forward flight and conversion mode ( $V = 0$  to 140 knots) the constant coefficient approximation to the dynamics is used. There is considerable variation of the dynamic stability in the conversion range, due to the change in the orientation of the rotor with respect to the wing. Also shown in this speed range are a number of points from the correct periodic coefficient solution. The periodic coefficient roots and the results of the constant coefficient approximation are nearly identical. This conclusion holds for all the roots of the system, although the high frequency rotor roots (not plotted) exhibit somewhat greater differences than do the wing and low-frequency rotor modes.

It is concluded that the periodic coefficients have only a small influence on the proprotor dynamics, as expected from the low value of the maximum advance ratio achieved. The constant coefficient approximation is quite adequate for tilting proprotor aircraft dynamics in helicopter-forward flight and conversion-mode operation. This conclusion should be checked for other applications, however, especially for operation in extreme flight conditions or with dynamic characteristics considerably different from the present case.

The calculation of the dynamic stability in nonaxial flight requires increased computation time compared to that for the axial flow cases, the increase is by a factor of about 4 for the constant coefficient case and by a factor of about 20 for the periodic coefficient case (for the present example). The principal increase is in calculating the aerodynamic coefficients around the rotor azimuth for the nonaxial flow cases. Using the constant coefficient approximation therefore allows a reduction in the computation time by a factor of about 5 for this example, with little loss of accuracy. Probably more important, however, is that with the constant coefficient approximation, the powerful analysis techniques available for time-invariant linear differential equations are applicable.

## RESULTS AND DISCUSSION: HINGELESS ROTOR

In this section the dynamic stability of the hingeless rotor is examined. We begin with a presentation of the blade bending and torsion modes, which were calculated by the methods described in reference 2 from the blade mass and stiffness distributions given in appendix A. Figure 21 shows the natural frequencies of the bending modes of the hingeless rotor blade as a function of forward speed for cruise mode rotor speed ( $\Omega = 386$  rpm). Figure 22 shows the tip deflection of the first three bending modes. The first mode is predominantly inplane motion, and the second predominantly out of plane. There is some flap/lag coupling of the modes, but it is small because the blade has nearly equal beamwise and chordwise bending stiffness at the root. Figure 23 shows typical bending mode shapes, at  $V/\Omega R = 0.7$ : the radial variation of the inplane ( $x$ ) and out-of-plane ( $z$ ) components of the bending deflections. Figure 24 shows the mode shapes and frequencies for the blade uncoupled rigid-pitch and elastic-torsion motion. The first mode is rigid pitch of the blade, due to control system flexibility, with a natural frequency of 5.3/rev. The higher modes are elastic torsion of the blade with no motion at the pitch bearing. The rigid pitch and first elastic torsion modes combine in the dynamics to give a coupled mode which is composed of about 60 percent rigid and 40 percent elastic motion, with a natural frequency of 4.5/rev. Figure 25 gives the trim deflection of the first two bending modes, for windmilling ( $C_Q = 0$ ) and powered (cruise  $C_T$ ) operation of the rotor in airplane cruise mode. There is negative elastic coning in both powered and windmilling operations, because of the low loading of the rotor in cruise flight. The rotor precone of  $2.5^\circ$  was chosen for the high loading of hover and hence is too high for cruise.

### Standard Case

The basic dynamics of the hingeless rotor and wing are shown in figure 26, which is a root locus for a velocity sweep from 100 to 500 knots. The case shown is a windmilling rotor with no blade-torsion dynamics. Figure 27 presents the variation with speed of the damping ratio of the three wing modes ( $q_1$ ,  $q_2$ , and  $p$ ) and the low-frequency rotor flap mode ( $\beta - 1$ ). The  $\beta - 1$  mode becomes unstable at high speed, giving a stability boundary at  $V = 470$  knots. By the time the instability occurs, this mode has assumed the character of a wing vertical bending mode (the  $q_1$  and associated  $p$ ,  $\xi_{1c}$ ,  $\xi_{1s}$ , and  $\psi_s$  motions). With this soft-inplane rotor ( $\nu_\xi < 1/\text{rev}$ ) the proximity of the  $\xi - 1$  and  $q_1$  mode frequencies significantly reduces the wing mode damping at low speeds. This effect is the air resonance phenomenon. A similar influence occurs with the high-speed resonance of the  $\xi - 1$  and  $q_2$  modes, leading to an instability of the wing chordwise bending mode (which can occur because the wing chordwise bending mode aerodynamic damping remains low even at high speed). The dynamic behavior of this rotor is discussed further in reference 1. Figure 27 also shows the predicted wing vertical bending mode damping compared with the results of a full-scale test of the hingeless rotor in the NASA-Ames 40- by 80-Foot Wind Tunnel (ref. 1).

Figure 28 further illustrates the air resonance behavior of this rotor; given is the variation of the wing vertical bending-mode damping ratio with rotor speed, for  $V = 50$  to 192 knots. At low speed (50 knots), the resonance of the  $\xi - 1$  and  $q_1$  mode frequencies actually leads to an instability of the wing vertical bending mode. At higher speeds, the reduction in the  $q_1$  damping due to air resonance is still present, but the increase with flight speed in the rotor lag aerodynamic damping and the wing vertical bending aerodynamic damping has been sufficient to stabilize the motion even at resonance. Figure 29 compares the predicted air resonance behavior with the full-scale test

results. Reasonable correlation is shown between the predicted and measured stability, except at the higher speeds where the tunnel turbulence made it difficult to extract the damping ratio from the experimental transient wing motion (see ref. 1).

### Elements of the Analytical Model

Figure 30 shows the influence of constant rotor speed operation and of omitting the wing aerodynamics for the hingeless rotor. As for the gimbaled rotor, the rotor rotational speed degree of freedom (dropped for the constant rotor speed case) and the wing aerodynamic forces have a significant role in the proprotor and wing dynamics. The influence of the trim bending deflection of the blade was examined, by setting it to zero in the calculations. Negligible effect was found (for this case with no blade-torsion motion), so the results are not plotted.

Figure 31 shows the effects of using uncoupled, rigid-blade bending modes, and of using only the  $c_{l\alpha}$  terms in the rotor aerodynamics. Both elements of the analytical model significantly influence the predicted dynamic stability. Figure 32 shows the effect of using both uncoupled bending modes and only the  $c_{l\alpha}$  terms in the rotor aerodynamics, which recovers the standard case of reference 1. Figure 33 shows the effect of using three bending modes per blade, compared with the standard case of two bending modes (a six-degree-of-freedom model for the rotor). Using three bending modes produces little improvement of the predicted dynamic stability.

### Blade Torsion

Now the influence of the blade rigid-pitch and elastic-torsion degrees of freedom on the proprotor and wing dynamics will be examined for the hingeless rotor. Figure 34 presents a root locus of a velocity sweep from 100 to 400 knots for a windmilling rotor including the blade torsion dynamics. Compared with the no-torsion results (fig. 26), there is a substantial influence of the blade-torsion degrees of freedom on both the wing and rotor modes. Figure 35 shows the effect of the torsion motion on the damping ratio of the wing modes. Compared with the results without torsion, there is a significant reduction in the dynamic stability at high speed due to the blade pitch motion. The addition of the torsion degrees of freedom changes the character of the wing vertical-bending ( $q_1$ ) mode, which now goes unstable at high speed. The  $q_1$  mode instability is above the low-frequency flap ( $\beta - 1$ ) mode instability, however, and the stability boundary for this case is not influenced. The effect on the wing torsion ( $p$ ) mode is not a change in its character but rather a substantial decrease in the speed for instability (compare the two root locus diagrams). The critical stability speed is reduced for all modes by the addition of the torsion dynamics. For the complete system, the stability boundary is reduced from about 470 knots to about 380 knots. There is also (for this case) a shift in the critical mode from  $\beta - 1$  for no torsion, to the wing chordwise bending ( $q_2$ ) mode with torsion. There is little difference between the results using one, two, or three torsion modes. Thus the effects of the torsion dynamics are primarily caused by first mode (the rigid-pitch degree of freedom). It is concluded that the blade-pitch degrees of freedom should be included in the analytical model of this hingeless rotor. A satisfactory model for the proprotor is at least nine degrees of freedom: the rigid pitch mode and two bending modes per blade.

Figure 36 examines the influence of the rotor trim bending deflection, by setting it to zero in the calculations. The effects are substantial with the blade-torsion degrees of freedom included

(recall that negligible effect was found for the no-torsion case), as might be expected from the significant trim coning and lag deflection of this hingeless rotor (fig. 25). Figure 36 also shows the calculated stability using the quasi-static approximation for the torsion dynamics. For this rotor the quasi-static approximation is not very successful as a representation of the effects of torsion. Figure 37 compares the predicted stability using two or three bending modes per blade, with the torsion dynamics now included. There is little effect of the third bending mode even with the blade-torsion motion included.

### Periodic Coefficients

The effect of the periodic coefficients on the hingeless proprotor dynamics in nonaxial flight (helicopter-forward flight and conversion-mode flight) will now be examined. Figure 38 shows the variation of the operating parameters along the flight path considered. Starting from hover, helicopter-mode operation extends to 80 knots. The pylon angle is converted to horizontal for  $V = 80$  to 140 knots. For this rotor the rotational speed is programmed with pylon tilt angle (in order to maintain sufficient air resonance mode stability), so the rotor speed is reduced from 551 to 386 rpm for  $V = 110$  to 140 knots. The flaps are raised in airplane mode from 140 to 160 knots; airplane-mode cruise then extends to 300 knots.

Figure 39 shows the damping ratio of the three wing modes along this flight path. The analytical model used is the proprotor and cantilever wing, with a constant rotor speed (powered operation) and no blade-torsion motion. In helicopter-forward flight and conversion mode ( $V = 0$  to 140 knots) the constant coefficient approximation to the dynamics is used. Also shown in this range are a number of points from the periodic coefficient solution. As for the gimbaled rotor, the periodic coefficient roots and the results of the constant coefficient approximation are nearly identical. The small influence of the periodic coefficients on the proprotor dynamics is the result of the low value of the maximum advance ratio achieved (about  $\mu = 0.2$ ). It is concluded that the constant coefficient approximation is an adequate representation of the tilting proprotor aircraft dynamics in helicopter-forward flight and conversion-mode operation.

## CONCLUSIONS AND RECOMMENDATIONS

Based on applications of the proprotor and wing theory developed in reference 2, the following conclusions are reached about the analytical model required for the accurate prediction of tilting proprotor aircraft dynamics.

The basic rotor dynamics were found to be satisfactorily described by a nine-degree-of-freedom model: two bending modes and the rigid-pitch mode per blade (including the gimbal and rotational-speed degrees of freedom as appropriate). Additional bending or torsion modes may be useful, however, to improve some of the details of the representation of the basic dynamics. This model of the rotor motion was arrived at both for the gimbaled rotor and for the hingeless rotor examined in this report, despite their quite different dynamic characteristics. Hence it is expected that this is a general conclusion for proprotor dynamics, regardless of the rotor type involved.

Comparing the behavior of the gimbaled, stiff-inplane rotor and the hingeless, soft-inplane rotor, it is concluded that the placement of the natural frequencies of the blade bending – the fundamental flap and lag frequencies – has a great influence on the dynamics of the proprotor and wing. It follows that an accurate calculation of the blade bending mode frequencies is important. As shown in appendix B, the effect of the blade-pitch motion is sensitive to the calculated mode shape at the root, and to other details of the blade root and hub (such as precone, and bending flexibility inboard of the pitch bearing). Hence the mode shape calculation, and in general the representation of the root and hub configuration in the analytical model, are important factors in predicting the dynamic stability when blade-pitch degrees of freedom are involved.

Other elements determined to be important to the analytical model include: coupled blade-bending modes, the rotor aerodynamic model, the blade-trim bending deflection (when the torsion motion is involved), the rotational-speed degree of freedom and its associated dynamics, and the wing aerodynamic forces. To this may be added the conclusion of reference 1, that an accurate structural dynamic model of the rotor support (here a cantilever wing) is also required. In general, it is desirable to use the best analytical model available, with as few simplifications as possible.

The constant coefficient approximation was found to be a satisfactory representation of tilting proprotor aircraft dynamics in nonaxial flow (where  $\mu > 0$ , i.e., operation in helicopter-forward flight or conversion-mode flight). This is a result of the low advance ratio (a maximum of  $\mu = 0.2$  in the present examples) characteristic of operation of the aircraft. However, for applications involving more extreme operating conditions the validity of this approximation should be rechecked.

### Recommendations

The analytical model should be extended to the complete vehicle, including the rigid body motions and the dynamics of the engine, drive-train, and governor. The cantilever wing configuration is suitable for a general investigation of the rotor model characteristics, but of course it provides no specific information on the aeroelastic stability level of a tilting proprotor aircraft. For the latter a model of the entire aircraft is required. Further experimental investigation of tilting proprotor dynamics is desirable, in particular investigation of the detailed characteristics such as have been examined in this report. The many programs of continuing work on hingeless rotor dynamics may be expected to benefit also the analysis of tilting proprotor aircraft.

Ames Research Center  
National Aeronautics and Space Administration  
and  
U.S. Army Air Mobility R&D Laboratory  
Moffett Field, Calif. 94035, Jan. 24, 1975

## APPENDIX A

### DESCRIPTION OF GIMBALLED AND HINGELESS PROPROPOTORS INVESTIGATED

The geometrical and structural characteristics of the two rotors examined in this report are presented in table 1 and figure 40. These are the data required by the analytical model of reference 2; the notation here follows that of reference 2.

The basic characteristics of the cantilever wing are also presented in table 1. The analytical model for the wing and pylon is developed in reference 2, and a complete list of the parameters used for that model is given in reference 1 (table 3, pp. 140-141). Representative airfoil properties, based on NACA 0012 section characteristics, were used for the rotor section aerodynamics (ref. 1, pp. 49-50). The following expression was used to calculate the kinematic pitch/bending coupling of the gimballed rotor:

$$K_{P_i} = \vec{i}_B \cdot \left[ 1.78 \vec{\eta}_i'(r_{FA}) - 15.9 \vec{\eta}_i(r_{FA}) \right]$$

(see ref. 2). The hingeless rotor had  $K_{P_i} = 0$  since the feathering axis was in the rigid hub.

The following parameters were used in the numerical calculation of the proprotor and wing dynamics:

1. Number of radial stations in integration of rotor aerodynamic forces = 9.
2. Number of radial stations in integration of rotor inertia forces (mode shapes) = 50.
3. Number of bending modes in calculation of rotor trim bending deflection = 2.
4. Parameters in calculation of blade modes (for a typical case, two bending modes and one elastic torsion mode): number of radial stations in integration of Galerkin coefficients = 40; number of functions in Galerkin solution for bending modes = 4; and number of functions in Galerkin solution for torsion modes = 2.
5. Parameters in calculation of aerodynamic coefficients for nonaxial flow (see ref. 2): constant coefficient approximation, number of azimuth points in average  $J = 12$  ( $\Delta\psi = 30^\circ$ ); periodic coefficient solution, azimuth increment in integration of equations  $\Delta\psi = 4^\circ$ .

## APPENDIX B

### ORIGIN OF THE BLADE PITCH MOTION EFFECTS

The origin of the effects of the blade-pitch dynamics observed for the gimballed, stiff-inplane rotor is primarily an effective pitch/lag coupling due to precone. This was determined by examining the magnitude of the terms in the differential equations for the pitch degrees of freedom. There are three dominant terms, all in the static (spring) matrix: the control system stiffness, the kinematic pitch/flap coupling, and an effective pitch/lag coupling due to precone. The following analysis gives the main features of this effect, although it is based on rigid, uncoupled bending modes. For further discussion of the role of the blade-pitch motion in rotor dynamics, see references 3 and 4.

The rotor blade in axial flight has a net flap moment on it, due to the aerodynamic and centrifugal forces on the blade (fig. 41a). When the blade lags, this flap moment has a component along the blade pitch axis, which must then be balanced by the control system stiffness:

$$(\text{net flap moment}) \zeta + (\text{control system stiffness}) \theta = 0$$

or

$$M_{\beta} \Delta \zeta + I_p \omega_{\theta}^2 \Delta \theta = 0 \quad (1)$$

where

$M_{\beta}$  net external flap moment/ $(\Omega^2 I_b)$

$I_p$  pitch moment of inertia/ $I_b$

$\omega_{\theta}$  pitch natural frequency (per rev)

There is also a pitch/flap coupling term, which is not considered for now. The effective pitch/lag coupling is then

$$K_{P_{\zeta}} = -\frac{\Delta \theta}{\Delta \zeta} = \frac{\text{net trim flap moment}}{\text{control system stiffness}} = \frac{M_{\beta}}{I_p \omega_{\theta}^2} \quad (2)$$

where  $K_{P_{\zeta}} > 0$  for lag back/pitch down. The normalized flap moment on the blade, due to the aerodynamic lift and centrifugal spring forces, is

$$M_{\beta} = \gamma \int_{ac}^L r dr - (\beta_p + \beta_{trim}) \quad (3)$$

where  $L$  is the blade section lift,  $\beta_p$  the precone angle, and  $\beta_{trim}$  the trim elastic coning deflection of the blade. Then the coupling is

$$K_{P\zeta} = - \frac{\beta_p + \beta_{trim} - \gamma \int \frac{L}{ac} r dr}{I_p \omega_\theta^2} \quad (4)$$

This effect is illustrated in figure 41(b). Due to the lag deflection  $\zeta r$ , the net force normal to the blade  $(\Omega^2 r m (\beta_p + \beta_{trim}) - L)$  produces a nose up moment about the pitch axis.

Some simplification of this result is possible, by considering the trim equilibrium of the flap moments. The rotor precone and blade lift produce a steady, elastic coning deflection of the blade, approximately:

$$\begin{aligned} \beta_{trim} &= \frac{1}{v_\beta^2} \left( \gamma \int \frac{L}{ac} r dr - \beta_p \right) \\ &\cong \frac{1}{v_\beta^2} \left( \frac{3}{4} \gamma \frac{C_T}{\sigma a} - \beta_p \right) \end{aligned} \quad (5)$$

where  $v_\beta$  is the natural frequency of the rotor coning mode. Then the effective pitch/lag coupling of the blade becomes:

$$K_{P\zeta} = \frac{(v_\beta^2 - 1) \beta_{trim}}{I_p \omega_\theta^2} \quad (6)$$

$$= - \left( \frac{v_\beta^2 - 1}{v_\beta^2} \right) \frac{\beta_p - \frac{3}{4} \gamma \frac{C_T}{\sigma a}}{I_p \omega_\theta^2} \quad (7)$$

If the rotor had ideal precone:

$$\beta_p = \beta_{p,ideal} = \gamma \int \frac{L}{ac} r dr$$

(which is the precone for no trim flap bending loads, i.e.  $\beta_{trim} = 0$ ), then there would be no pitch/lag coupling. In cruise, the proprotor operates at very low loading, however, while the precone is chosen for the high loading of hover. Hence the trim elastic coning angle  $\beta_{trim}$  is negative for the proprotor in cruise, and there is finite, negative effective pitch/lag coupling.

With ideal precone, the trim aerodynamic and centrifugal flap moments on the blade exactly balance, so there is no net moment to have a pitch component when the blade lags. With larger precone than the ideal value, as for the proprotor in cruise, the increased centrifugal flap moment must be balanced by a blade elastic moment due to coning. Consequently, negative  $\beta_{trim}$  is produced until a balance of coning moments is achieved again. Then there is a net external flap moment on the blade (balanced by an internal structural moment) which produces a pitch moment when the blade lags. A measure of this net external moment is  $\beta_{trim}$ , hence equation (6) for  $K_{P\zeta}$ .

In cruise, this gimballed rotor has low-loading and high-coning stiffness, so the effect of precone dominates. Equation (7) implies then

$$K_{P\zeta} \cong - \frac{\beta_p}{I_p \omega_\theta^2}$$

Hence, precone and control system stiffness are expected to be primary parameters in the effect of the blade-pitch motion on the proprotor dynamics. When other factors are included, which tend to reduce the coupling (the effect of  $\beta_{trim}$  and  $C_T$ , as well as coupled modes, center of gravity offset, etc.), a value of about  $K_{P\zeta} = -0.3$  is found for the effective pitch/lag coupling. This large pitch/lag coupling is the source of the substantial influence of the blade torsion degrees of freedom on the proprotor dynamics.

Figure 42 shows the influence of precone on the effects of the pitch dynamics. The wing vertical bending mode damping ratio is given for  $\beta_p = 2.5^\circ$  (the base value),  $1.5^\circ$ , and  $0^\circ$ , and compared with the no-torsion results. The effect of the reduced pitch/lag coupling for the smaller precone angles is evident. Figure 43 shows the effect of increasing the control system stiffness:  $\omega_\theta = 4.8/\text{rev}$  (the base value),  $7/\text{rev}$ , and  $10/\text{rev}$ . The no-torsion results is the case of infinite control-system stiffness, and also infinite blade-torsion stiffness. Increasing  $\omega_\theta$  decreases the coupling as expected. These figures confirm the major role of the precone and control system stiffness in the pitch dynamics, as suggested by the above analysis.

The calculations presented so far have been for a rotor with a pitch bearing radial location of  $r_{FA}/R = 0.09$ . With the bending modes used, there is little slope or deflection of the feathering axis associated with blade bending; in fact, the results are nearly the same as those obtained when it is assumed that the pitch bearing is rigidly fixed with respect to the hub ( $r_{FA} = 0$ ). The rough analysis given above for the effective pitch/lag coupling of the blade is based on the assumption that there is no lag-bending flexibility inboard of the pitch bearing. The blade-pitch dynamics are, however, very sensitive to inboard bending flexibility. Corresponding to the approximate derivation given above, the effect of the pitch bearing radial location is basically an additional factor in  $K_{P\zeta}$  of

$$(\eta/r) - \eta'(r_{FA})$$

where  $\eta(r)$  is the lag bending mode shape. Bending flexibility inboard of the pitch bearing increases the slope of the mode at the feathering axis,  $\eta'(r_{FA})$ , and thus reduces the effective pitch/lag coupling. Figure 44 examines the effect of inboard bending flexibility. The same bending modes are used, but the radial position of the pitch bearing is increased, which for these cantilever modes introduces lag-bending flexibility inboard of the feathering axis. Figure 44 presents the wing vertical-bending mode damping ratio for  $r_{FA}/R = 0.09$  (the base value),  $0.2$ , and  $0.3$ . The improvement in dynamic stability due to the reduced pitch/lag coupling as  $r_{FA}$  increases is evident. The following table gives the values of the bending mode slope at the pitch bearing, the effective pitch/lag coupling, and the stability boundary for these cases.

$r_{FA}$	$\eta' (r_{FA})^*$	$KP_{\zeta}^*$	$V_{crit}$ (knots)
0	0	-.31	310
.09	.15	-.31	310
.2	.39	-.21	330
.3	.64	-.01	380
no torsion	---	---	450

\*At  $V=250$  knots

The results for varying  $r_{FA}$  imply that the dynamic stability is sensitive to the lag-bending mode slope in the vicinity of the blade root, and especially to the distribution of bending flexibility inboard and outboard of the pitch bearing. It follows also then that the calculated stability must be sensitive to the bending-mode shape calculation. For most purposes, it is sufficient to obtain an accurate representation of the blade bending for outboard portions of the blade, where the aerodynamic, inertial, and centrifugal forces are high. When the pitch dynamics are involved however, accuracy is required also in the calculation of the mode slope at the root.

## REFERENCES

1. Johnson, Wayne: Dynamics of Tilting Proprotor Aircraft in Cruise Flight. NASA TN D-7677, May 1974.
2. Johnson, Wayne: Analytical Model for Tilting Proprotor Aircraft Dynamics, Including Blade Torsion and Coupled Bending Modes, and Conversion Mode Operation. NASA TM X-62,369, Aug. 1974.
3. Hodges, Dewey H.; and Ormiston, Robert A.: Stability of Elastic Bending and Torsion of Uniform Cantilevered Rotor Blades in Hover. AIAA Paper No. 73-405, March 1973.
4. Huber, H. B.: Effect of Torsion-Flap-Lag Coupling on Hingeless Rotor Stability. 29th Annual National Forum of the American Helicopter Society, Washington, D.C., May 9-11, 1973.

TABLE 1.— DESCRIPTION OF PROPROPOTORS CONSIDERED IN ANALYSIS

	Gimballed stiff-inplane rotor	Hingeless soft-inplane rotor
<b>Rotor</b>		
Number of blades	3	3
Radius, $R$ , m	3.81	3.96
Tip speed, $\Omega R$ , m/sec (cruise mode)	183	160
Rotational speed, $\Omega$ , rpm (cruise mode)	458	386
Lock number, $\gamma$	3.83	4.04
Flap inertia, $kg - m^2$ (used for $\gamma$ )	142	203
Rotor mass, $kg$ (blades and hub)	181	173
Solidity ratio	0.089	0.115
Chord	0.093 $R$	0.121 $R$
Pitch/flap coupling, $\delta_3$ , deg	-15	0
Precone, $\beta_p$ , deg	2.5	2.5
Pitch bearing offset, $r_{FA}$	0.091 $R$	0.06 $R$
Torque offset	0	0.0042 $R$
Extent rigid hub	0.02 $R$	0.07 $R$
Gimbal damping (percent critical)	0.1	---
Bending and torsion structural damping (percent critical)	0.5	0.5
<b>Wing</b>		
Semispan	1.333 $R$	1.281 $R$
Mast height	0.342 $R$	0.354 $R$
Typical frequencies (cruise mode)		
Vertical bending, per rev	0.42	0.36
Chordwise bending, per rev	0.70	0.62
Torsion, per rev	1.30	1.48

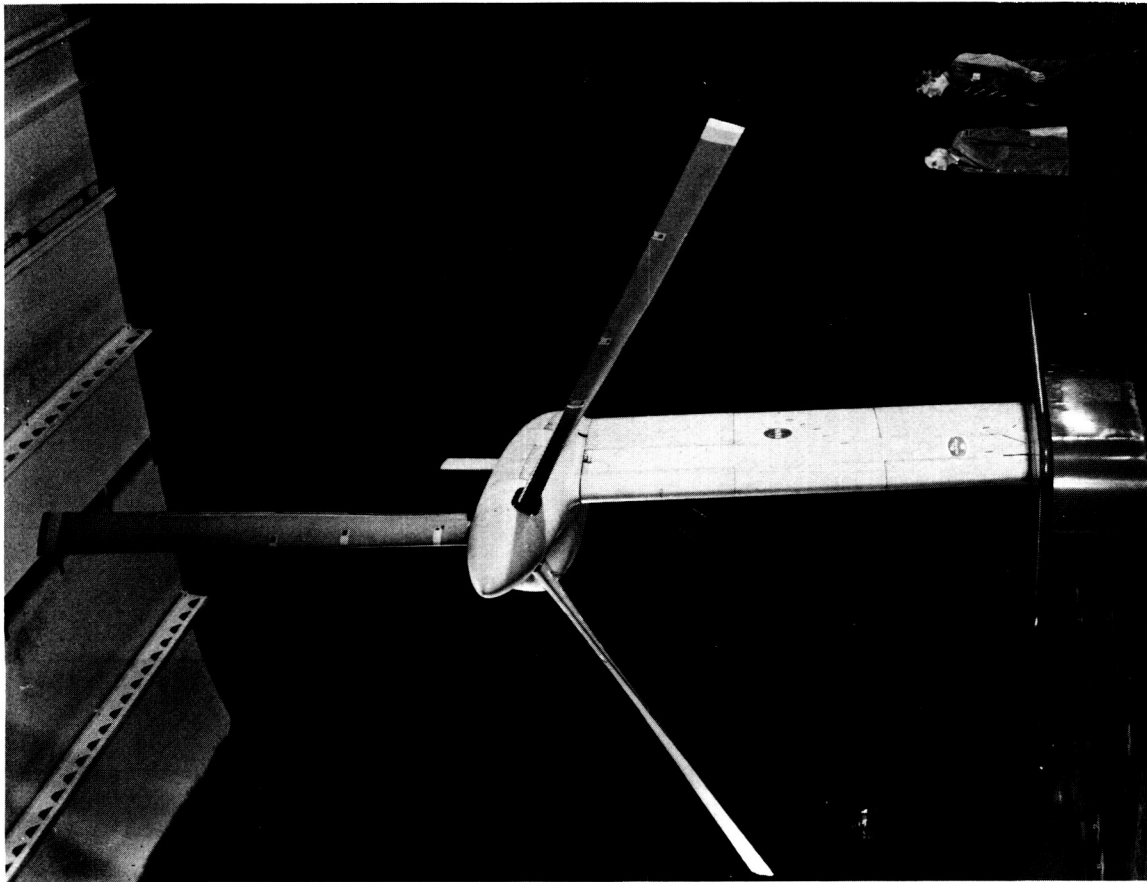


Figure 1.— Proprotor and cantilever wing configuration.

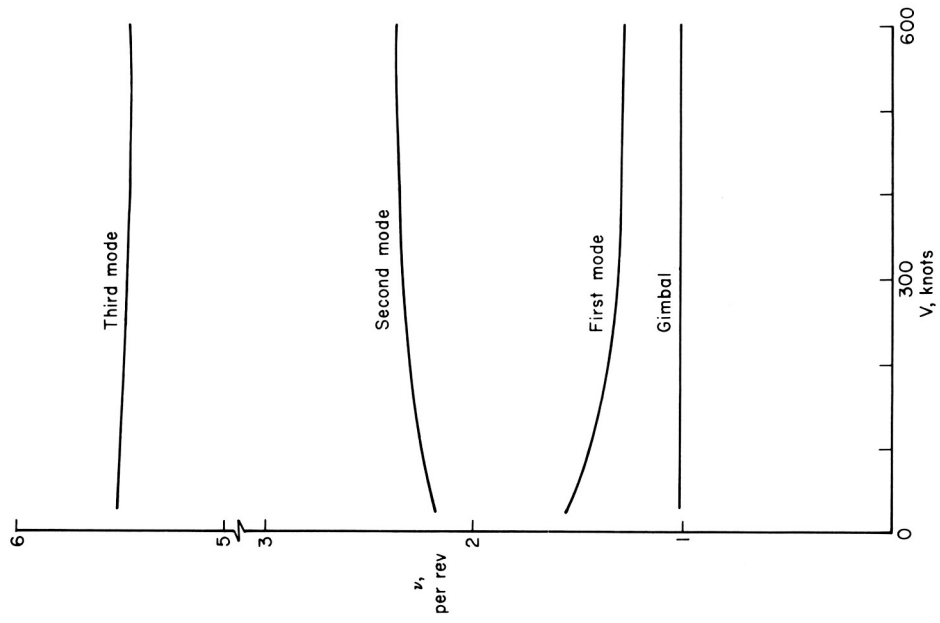


Figure 2.— Gimballed rotor: cantilever blade-bending mode natural frequencies at  $\Omega = 458$  rpm: gimbal-mode frequency also shown.

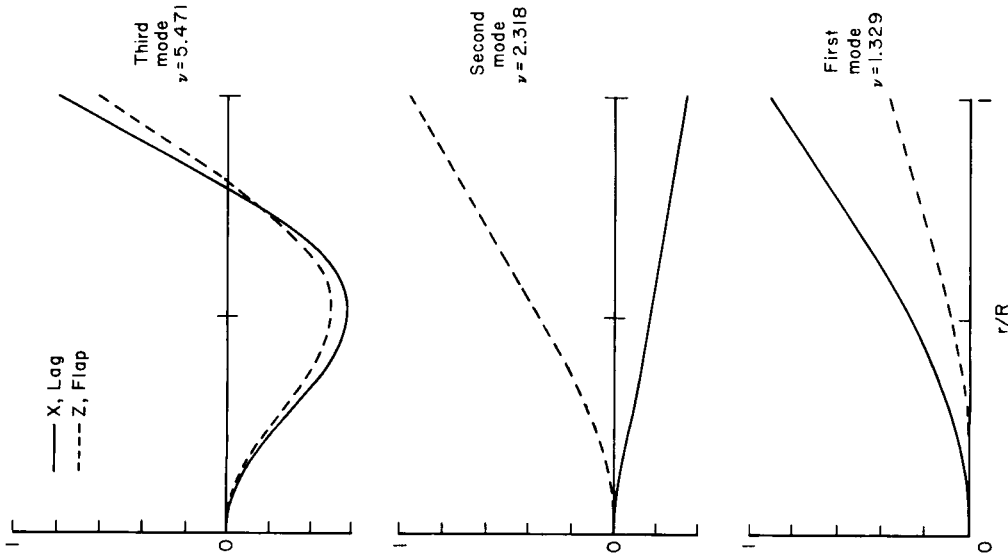


Figure 4.— Gimballing rotor: cantilever blade-bending mode shapes for  $V/\Omega R = 0.7$  and  $\Omega = 458$  rpm ( $V = 240$  knots and  $\theta_{.7s} = 44.3^\circ$ ).

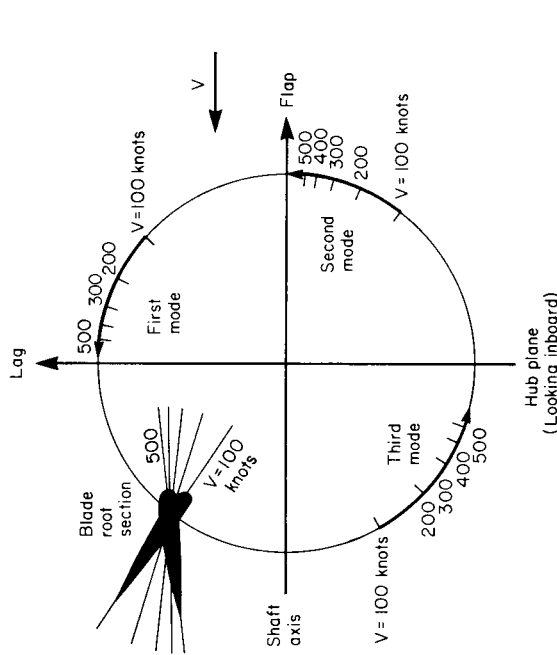


Figure 3.— Gimballing rotor: blade-bending mode tip deflection for  $\Omega = 458$  rpm and  $V = 100$  to 500 knots; orientation of blade root section also shown.

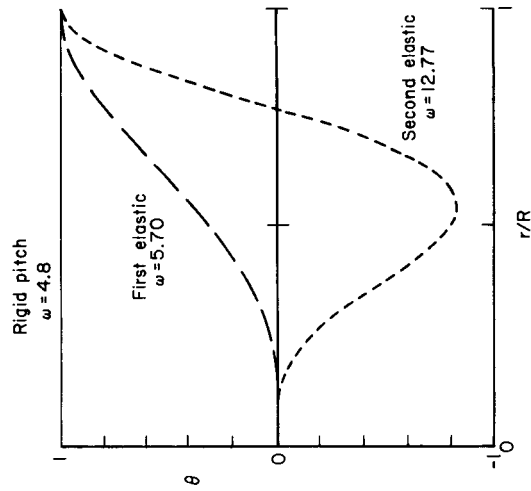


Figure 5.— Gimballed rotor: blade-torsion mode shapes and frequencies, for uncoupled rigid-pitch and elastic-torsion motion.

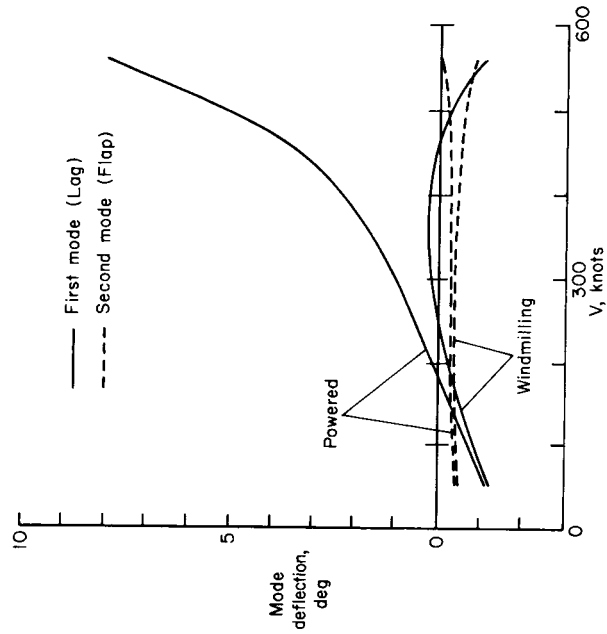


Figure 6.— Gimballed rotor: trim deflection of blade-bending modes, in degrees at the blade tip, for windmilling and powered operation ( $\Omega = 458$  rpm).

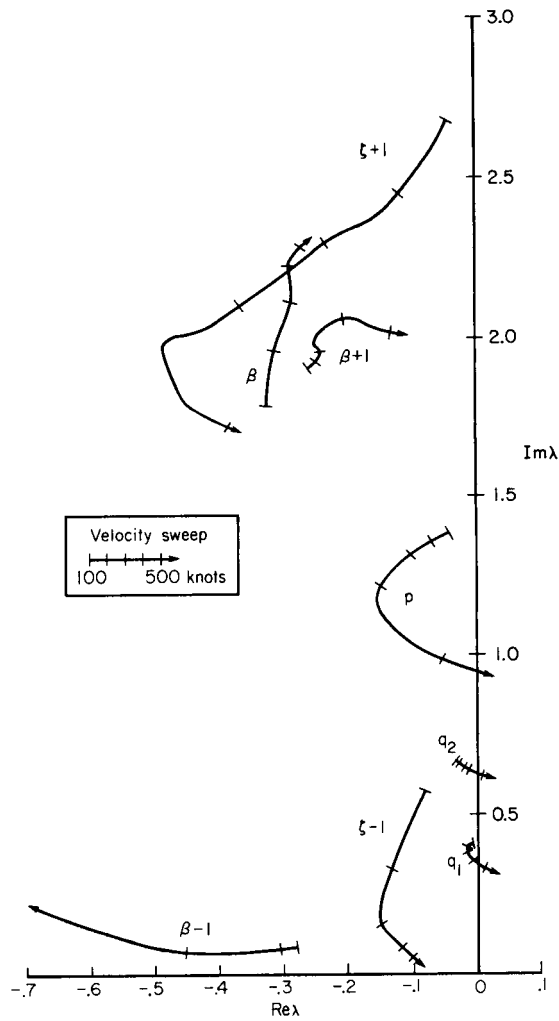


Figure 7.— Gimbaled rotor: root locus for velocity sweep at  $\Omega = 458$  rpm, windmilling rotor.

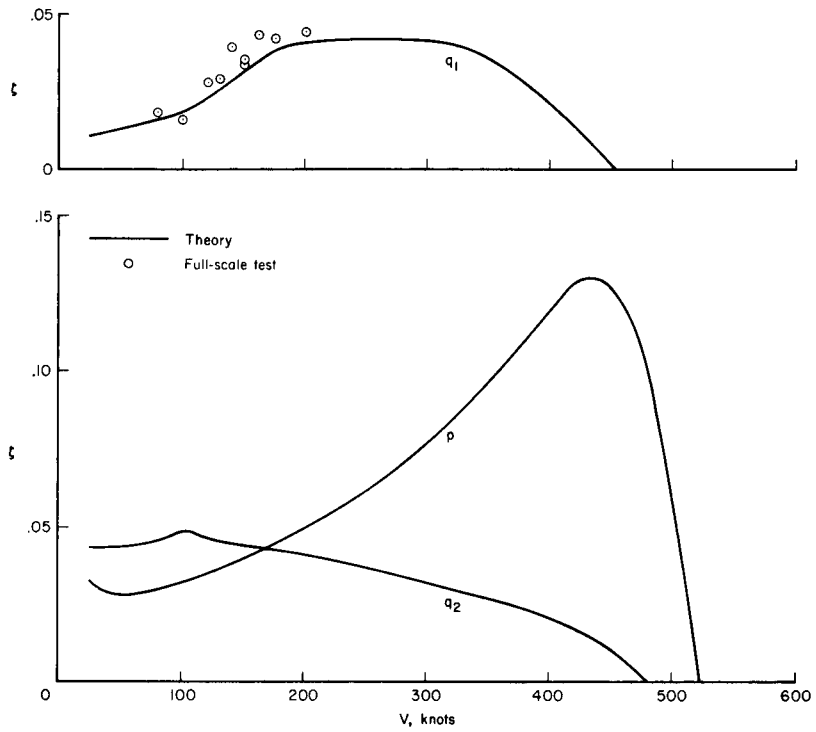


Figure 8.— Gimbaled rotor: damping ratio of wing modes, and comparison with full-scale test results.

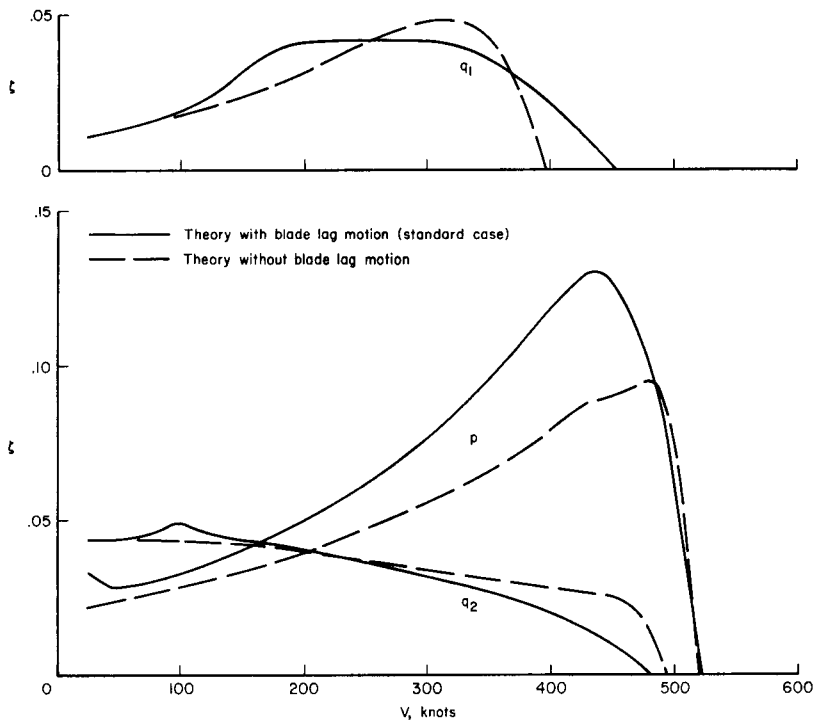


Figure 9.— Gimbaled rotor: effect of rotor-lag degrees of freedom.

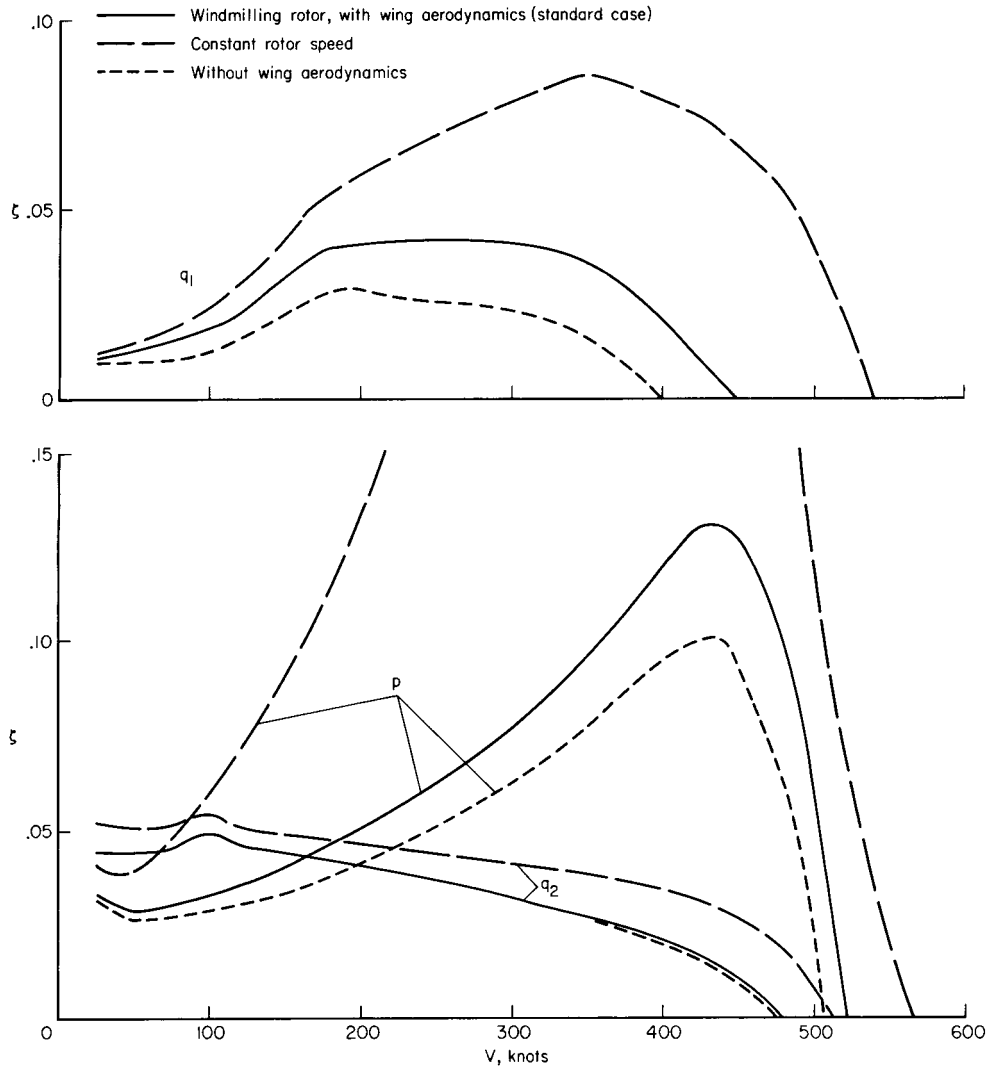


Figure 10.— Gimbaled rotor: effect of wing aerodynamics and rotor rotational speed perturbation (dropped for the constant rotor speed case).

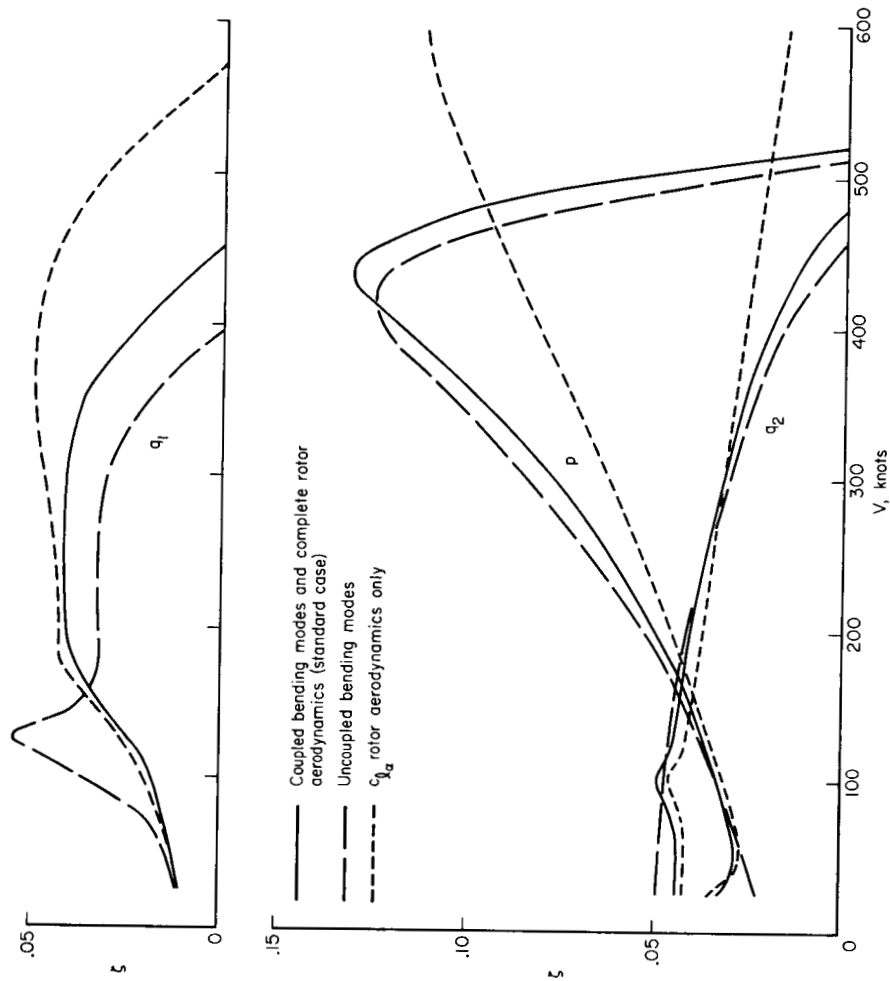


Figure 11.— Gimballed rotor: effect of uncoupled, rigid modes for blade-bending, and effect of using only  $c_1 \alpha$  terms in rotor aerodynamics.

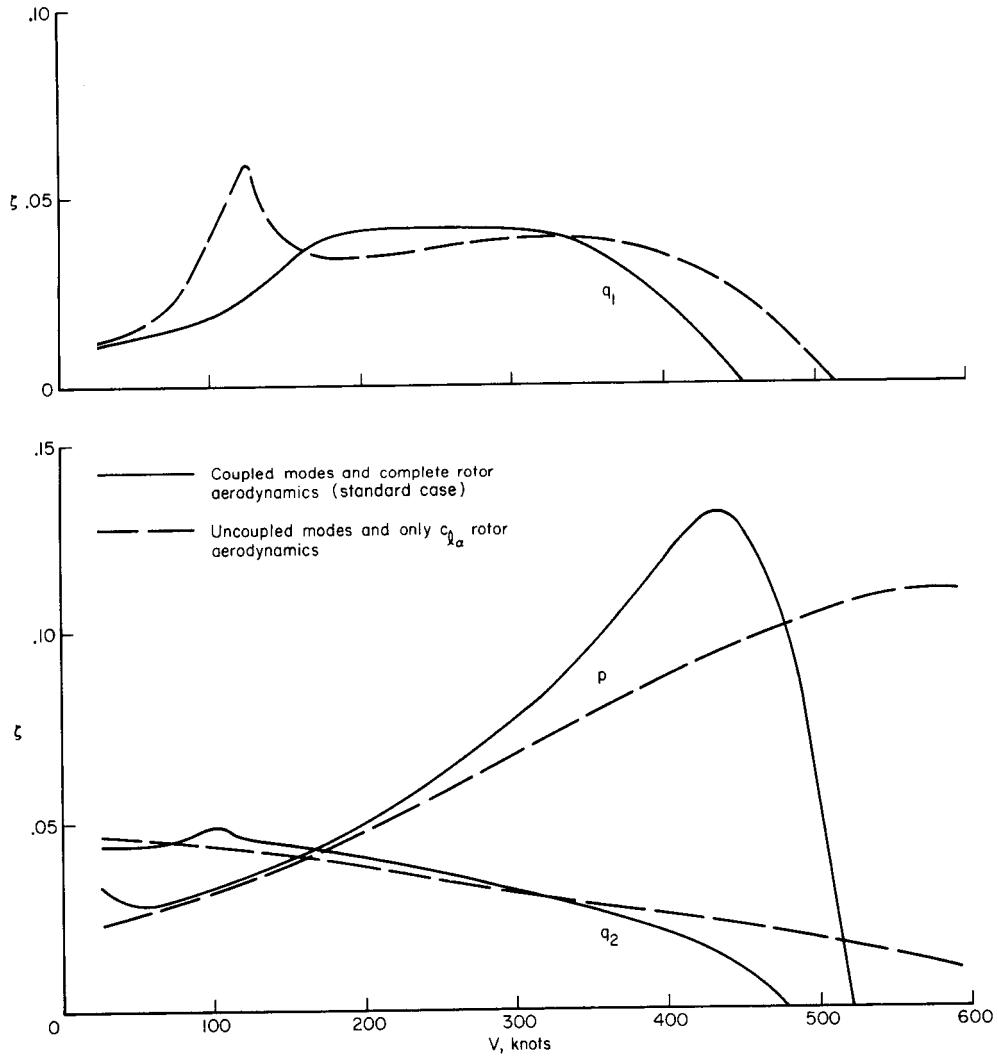


Figure 12.— Gimballing rotor: effect of using both uncoupled blade-bending modes and only  $c_{1\alpha}$  terms for rotor aerodynamics.

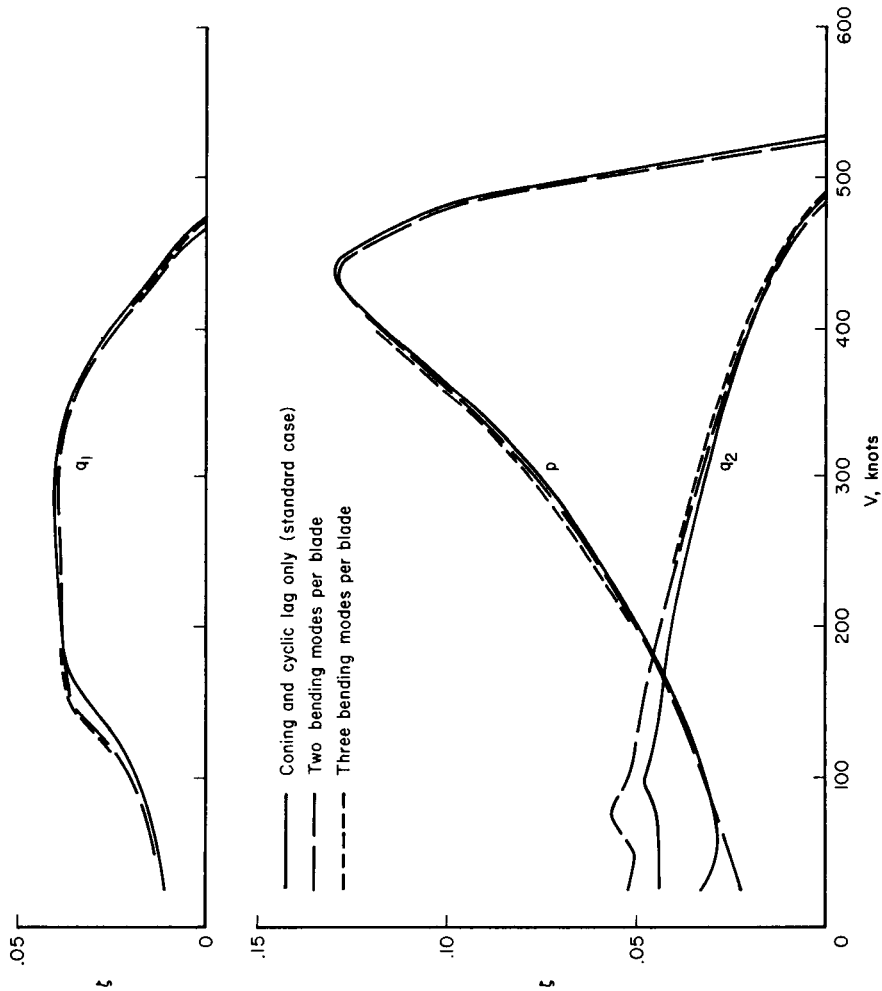


Figure 13.— Gimballed rotor: effect of using two or three bending-modes per blade, compared with using just the coning and cyclic-lag modes (base case).

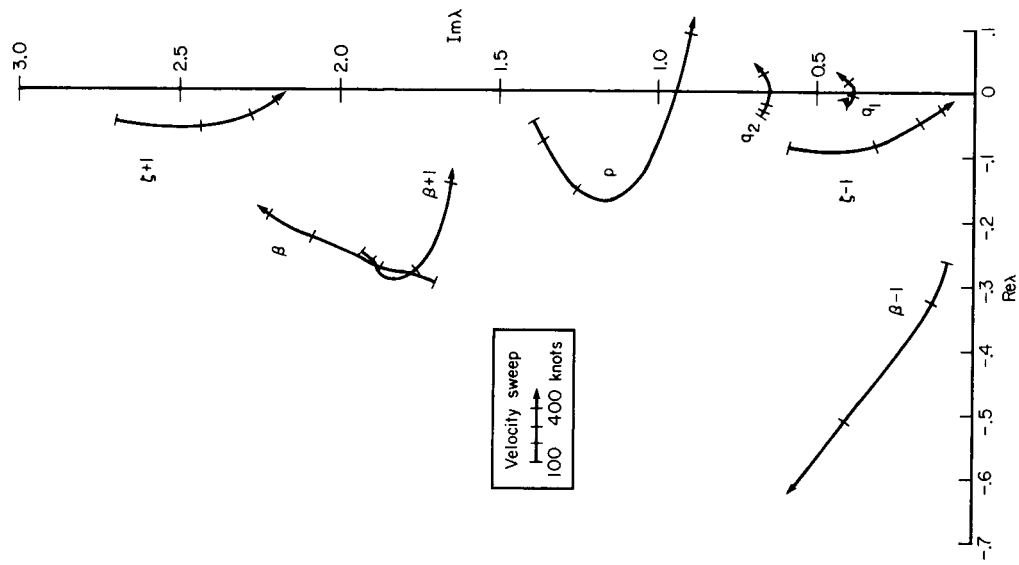


Figure 14.— Gimballed rotor: root locus for velocity sweep at  $\Omega = 458$  rpm windmilling rotor; including rotor blade pitch and torsion degrees of freedom.

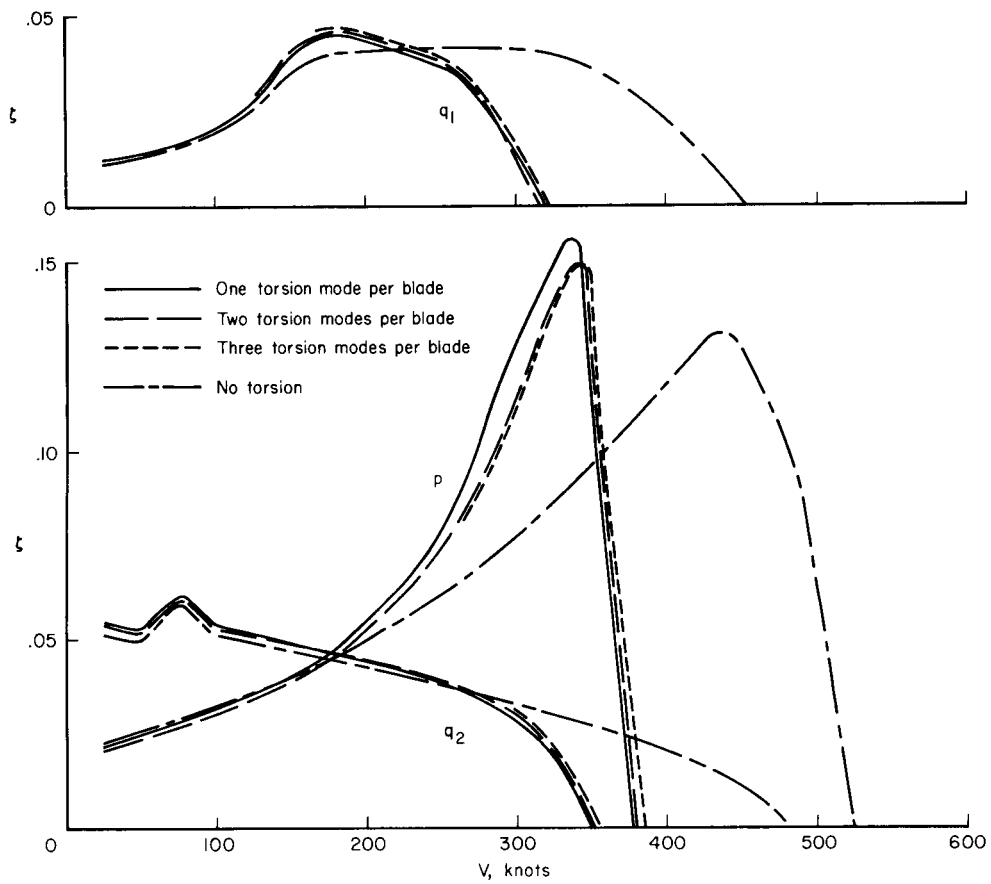


Figure 15.— Gimbal rotor: influence of rotor-blade torsion dynamics, comparing the damping ratio of the wing modes using one, two, three, or no torsion degrees of freedom per blade.

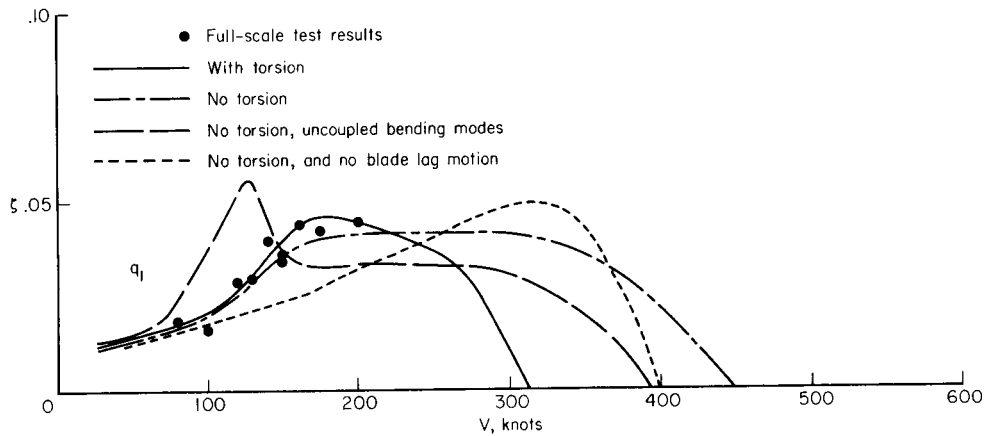


Figure 16.— Gimbal rotor: wing vertical bending-mode damping ratio, comparing results of several analytical models with full-scale test results.

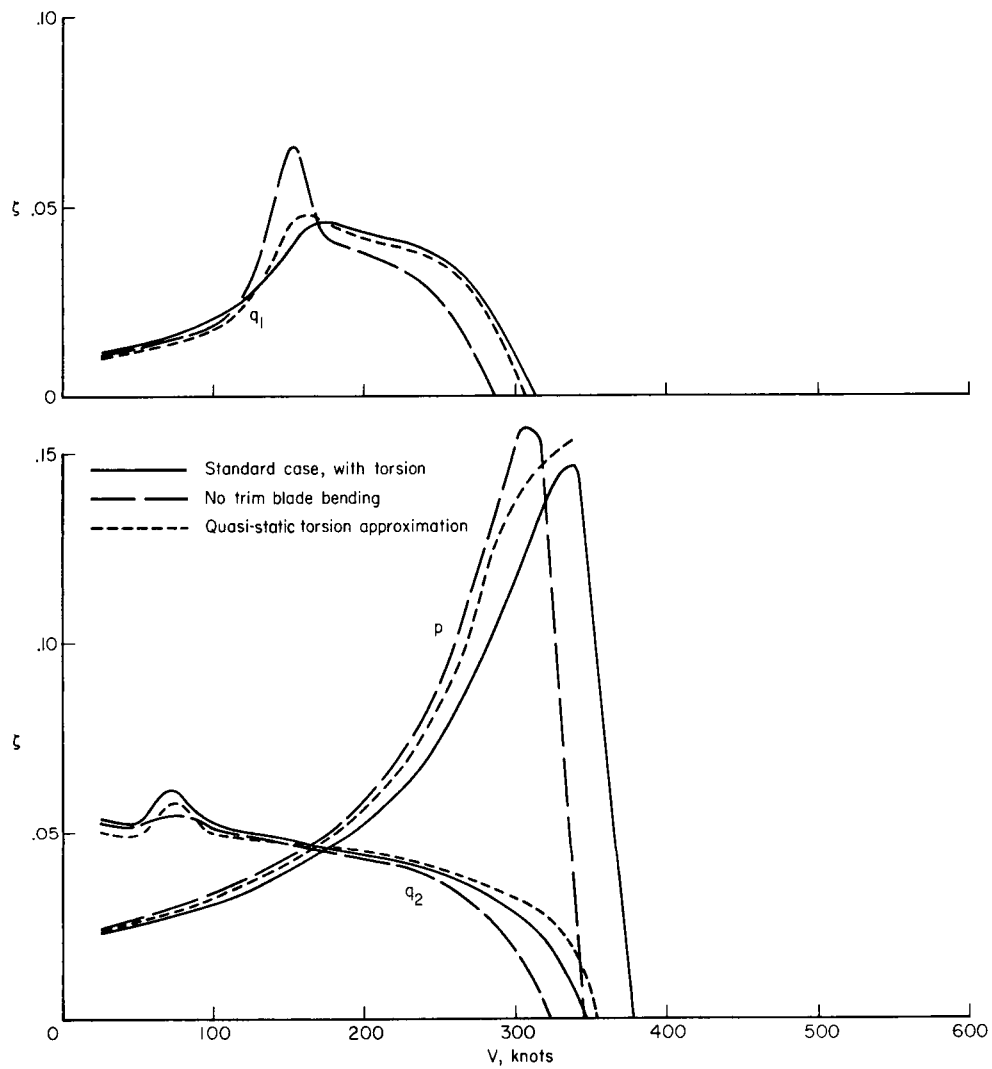


Figure 17.— Gimbaled rotor: wing-mode damping, showing influence of blade-trim bending deflection and of quasi-static torsion approximation when the blade-torsion dynamics are involved.

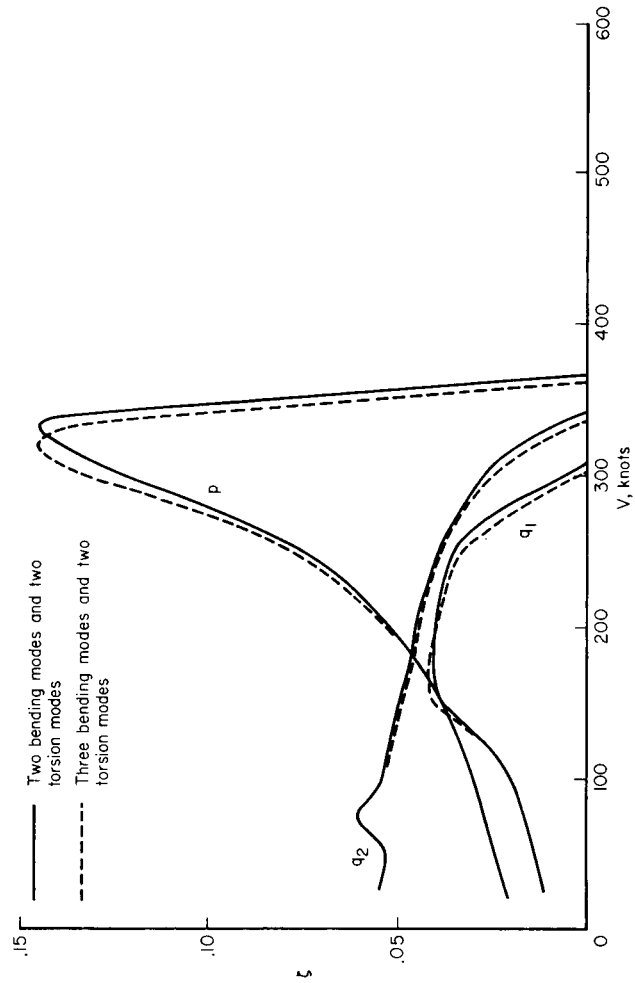


Figure 18.— Gimballed rotor: effect of using two or three blade-bending modes, including blade-torsion dynamics.

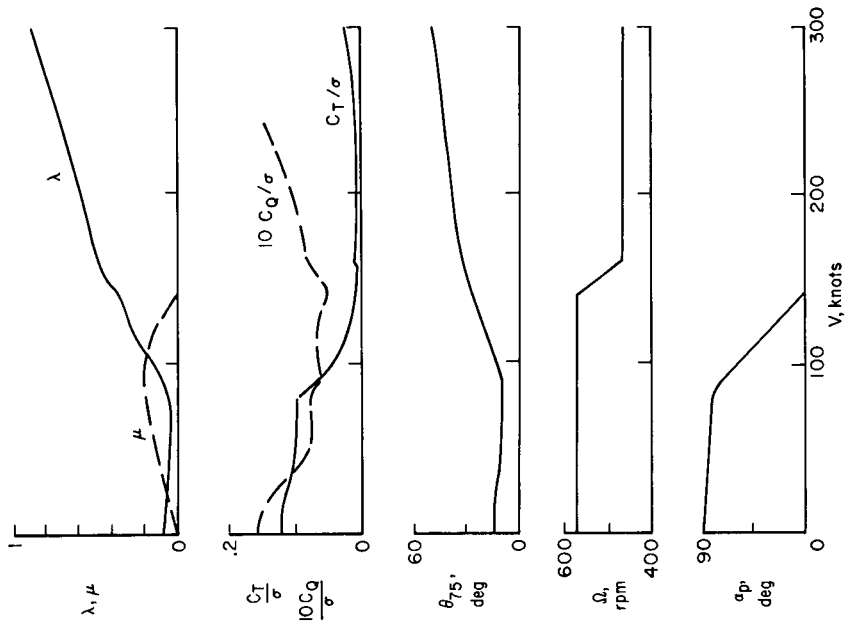


Figure 19.— Gimballed rotor: variation of parameters on flight path including conversion from helicopter-mode to airplane-mode operation.

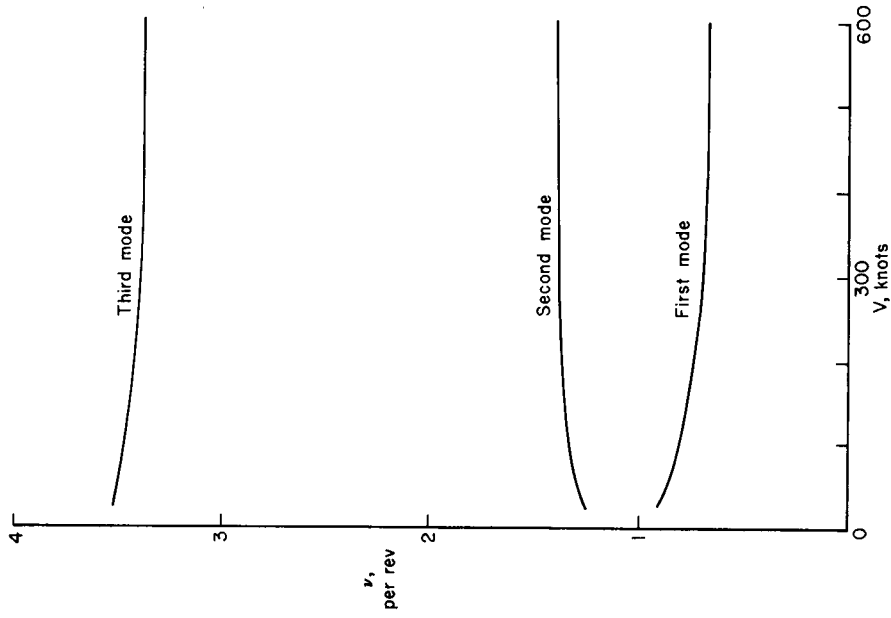


Figure 21.— Hingeless rotor: cantilever blade-bending mode natural frequencies, at  $\Omega = 386$  rpm.

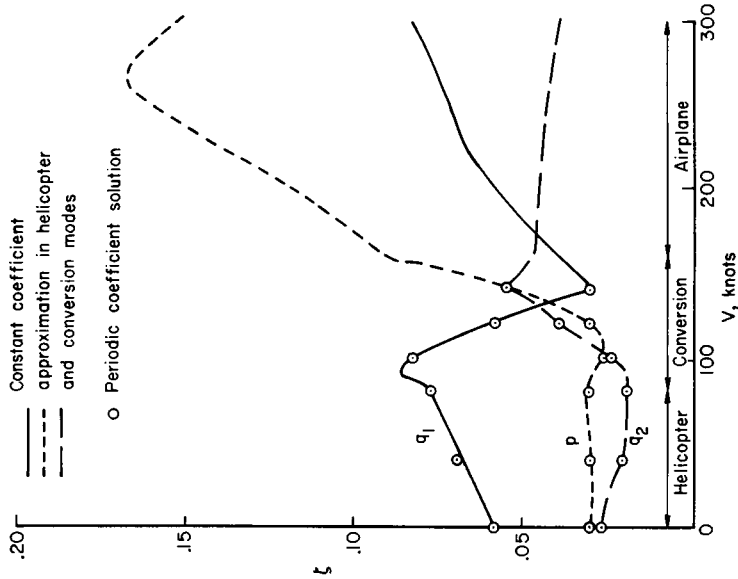


Figure 20.— Gimballed rotor: damping ratio of wing modes on flight path through conversion, comparing results of constant coefficient approximation with periodic coefficient solution.



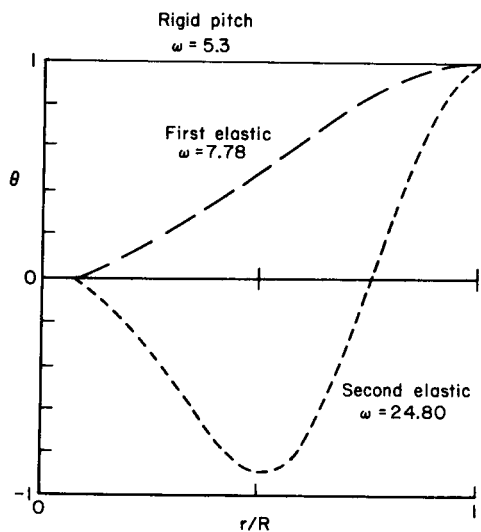


Figure 24.— Hingeless rotor: blade-torsion mode shapes and frequencies, for uncoupled rigid-path and elastic-torsion motion.

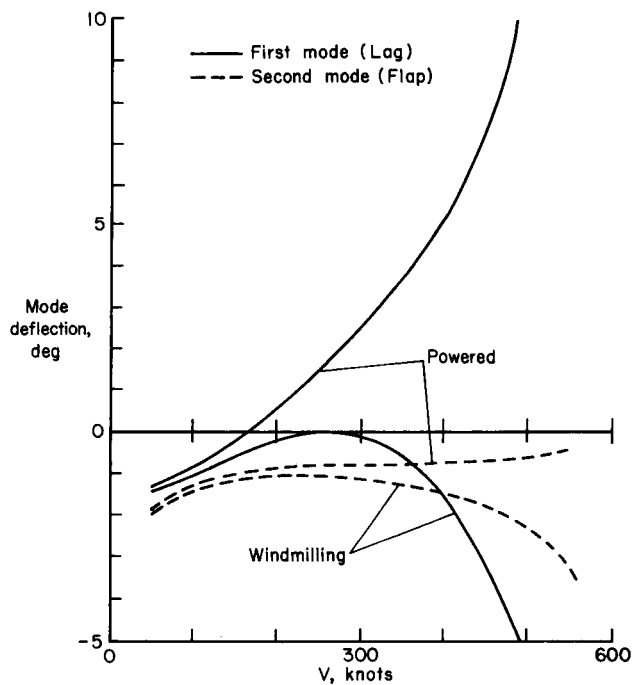


Figure 25.— Hingeless rotor: trim deflection of blade-bending modes, in degrees at the blade tip, for windmilling and powered operation ( $\Omega = 386$  rpm).

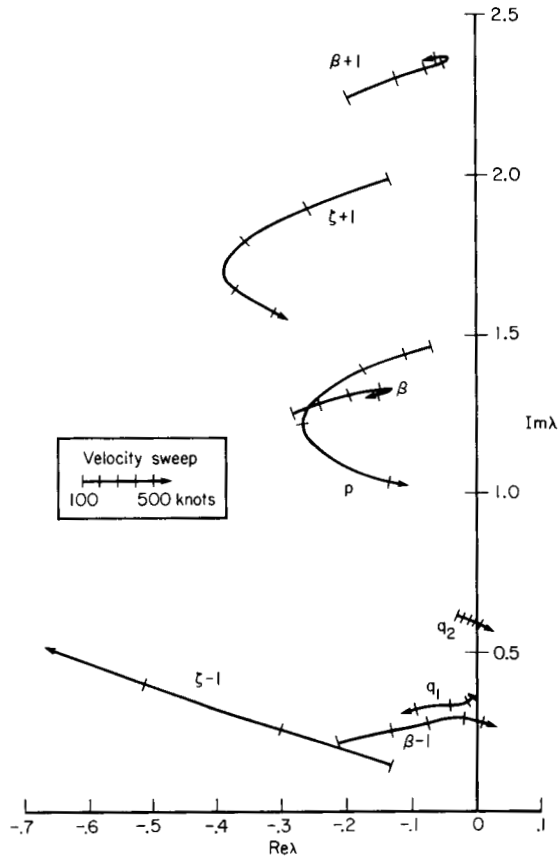


Figure 26.— Hingeless rotor: root locus for velocity sweep at  $\Omega = 386$  rpm, windmilling rotor.

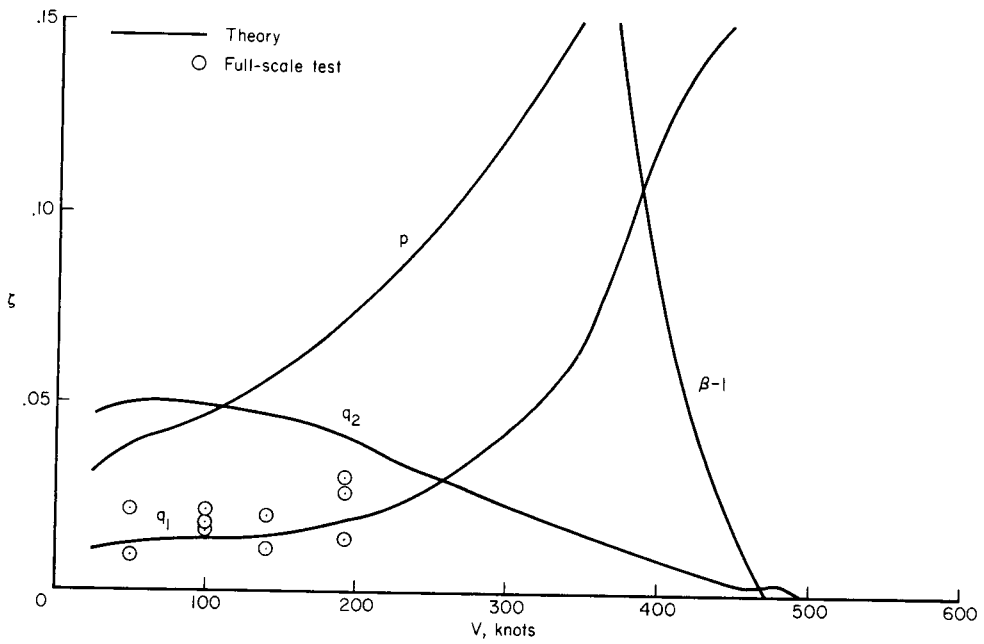


Figure 27.— Hingeless rotor: damping ratio of the wing and low-frequency flap modes, and comparison with full-scale test results (for  $q_1$  only).

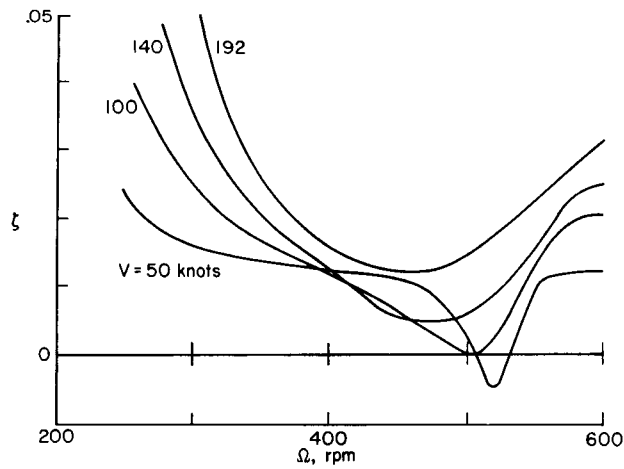


Figure 28.— Hingeless rotor: air resonance behavior. Variation of wing vertical bending-mode ratio with rotor speed for  $V = 50, 100, 140,$  and  $192$  knots.

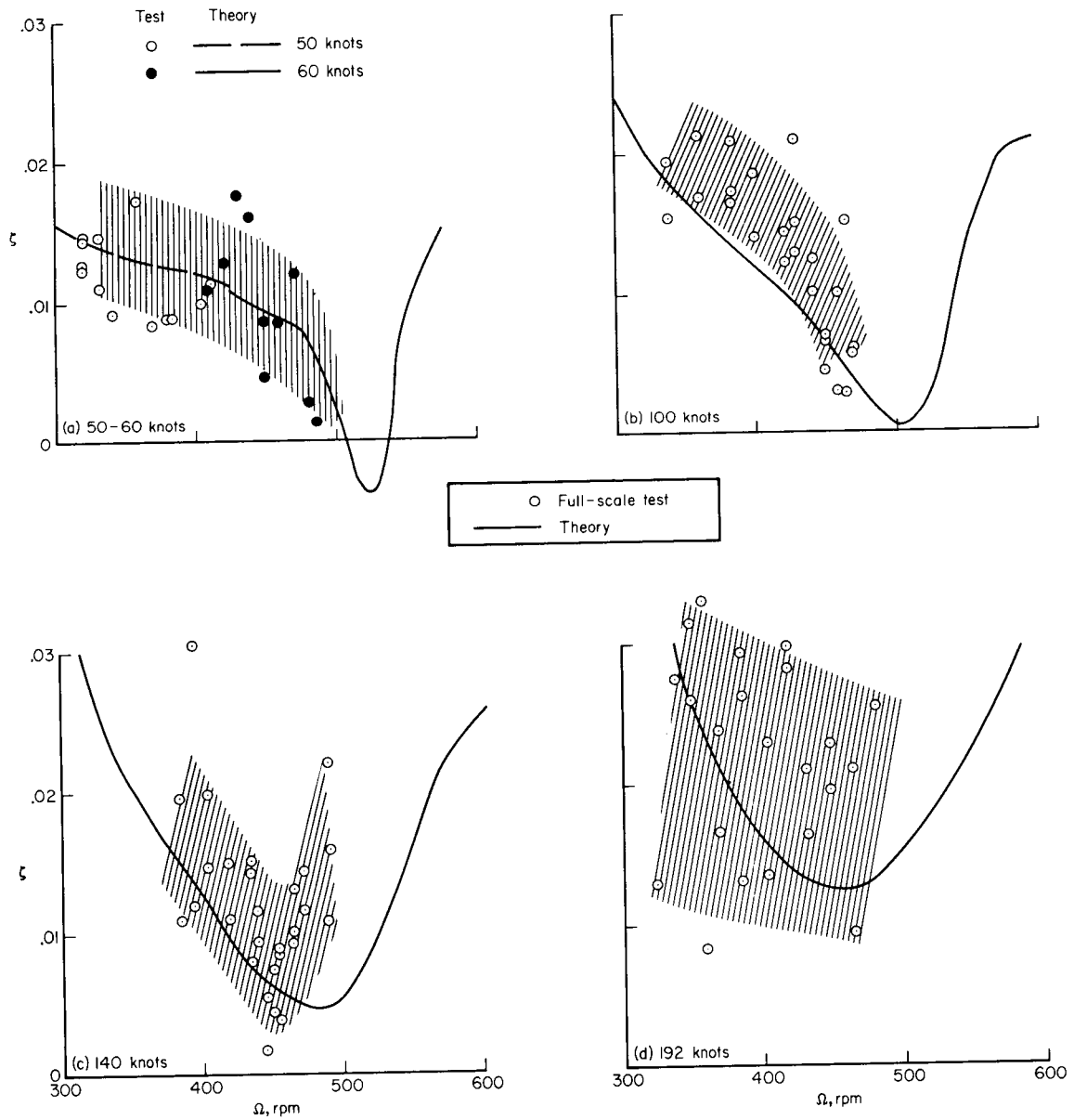


Figure 29.— Hingeless rotor: variation of wing vertical-bending mode damping ratio with rotor speed, and comparing with full-scale test results.

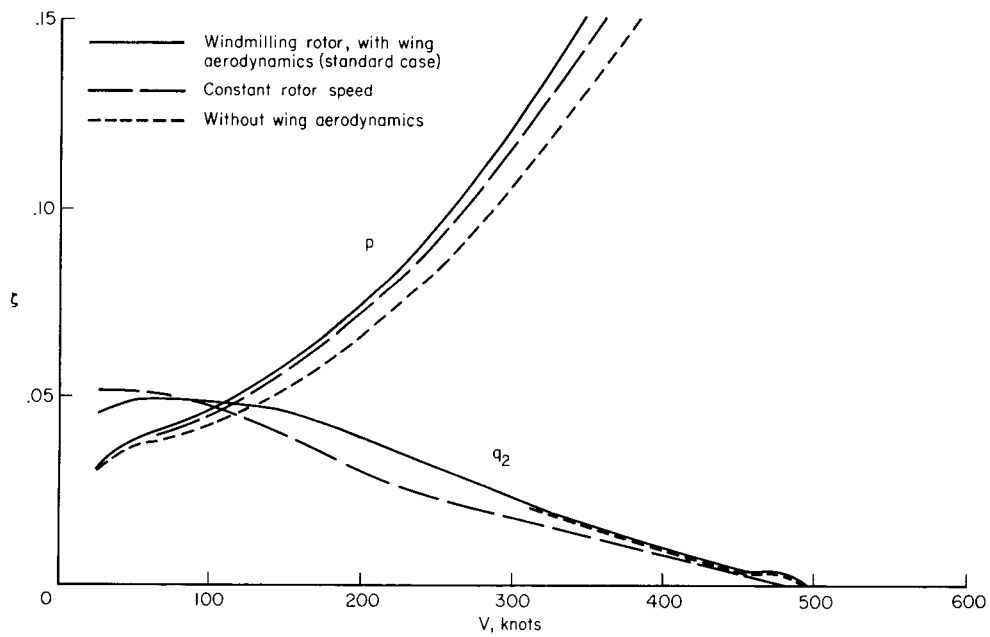
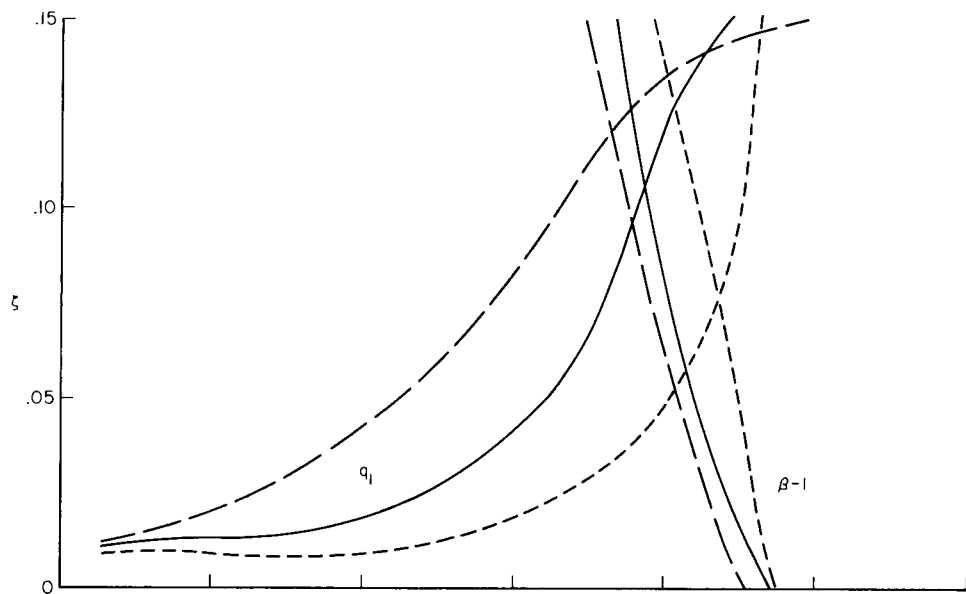


Figure 30.— Hingeless rotor: effect of wing aerodynamics and rotor rotational speed perturbation (dropped for the constant rotor speed case).

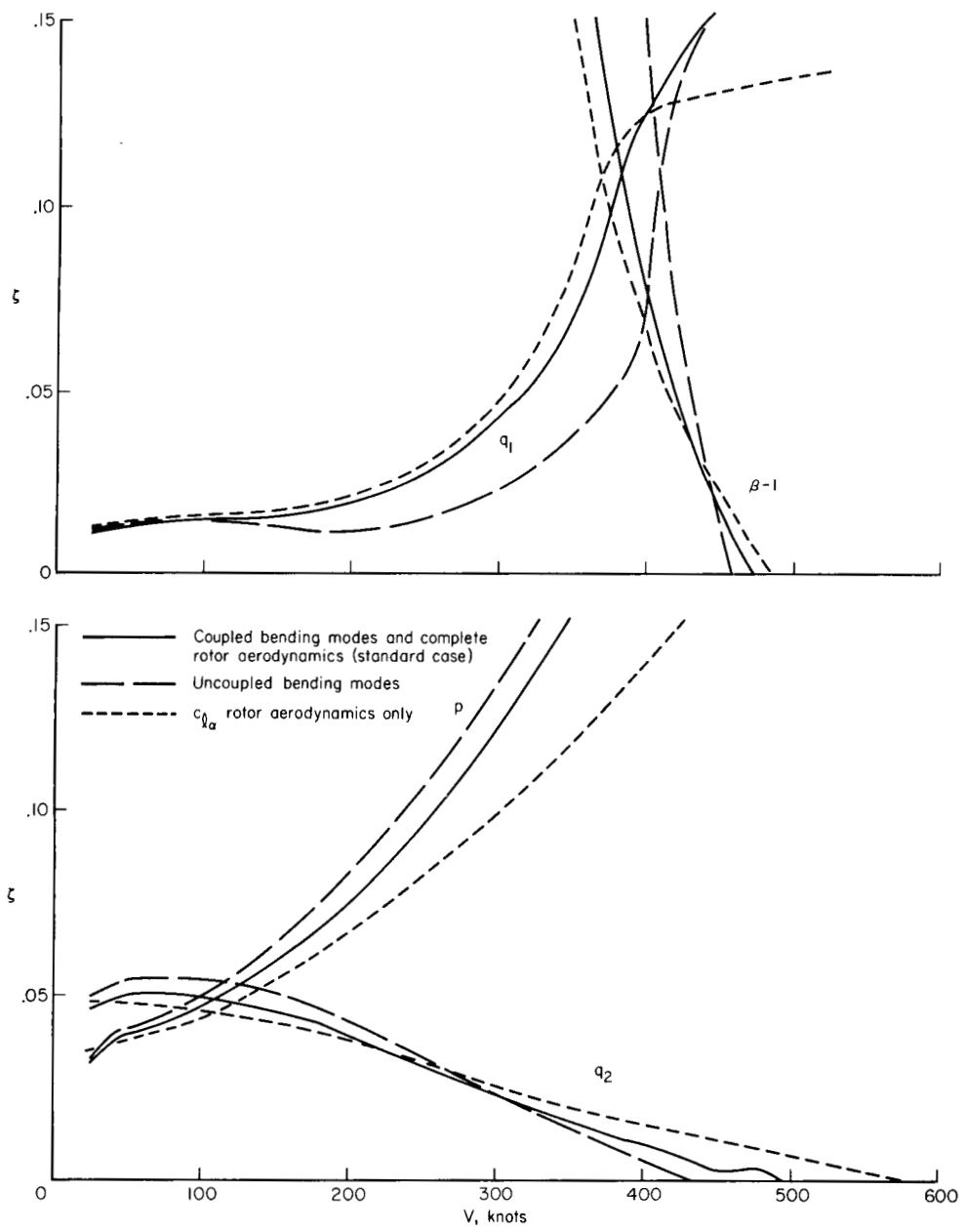


Figure 31.— Hingeless rotor: effect of uncoupled, rigid modes for blade bending, and effect of using only  $c_{1\alpha}$  terms in rotor aerodynamics.

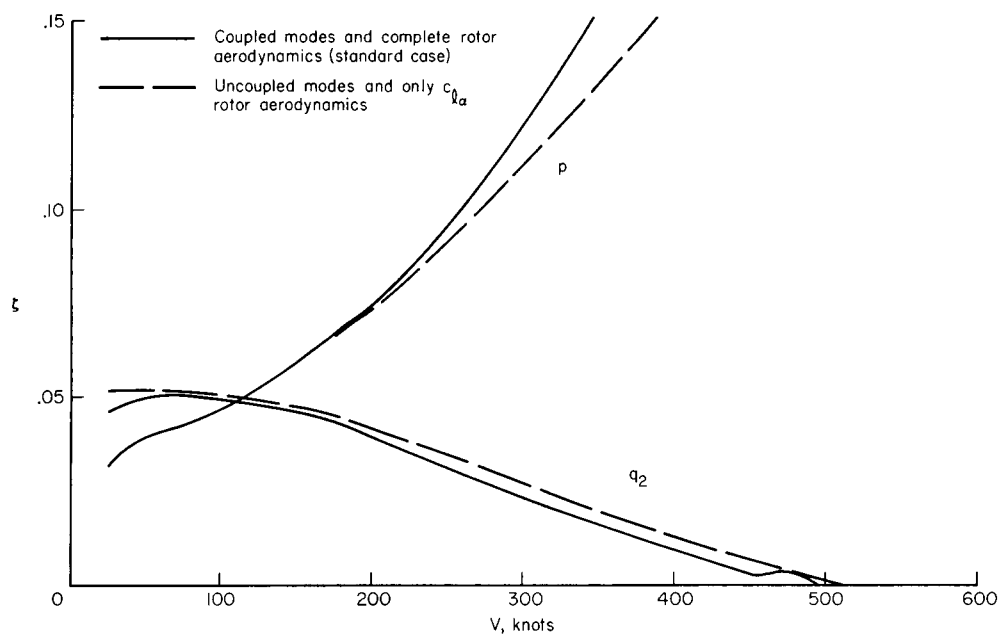
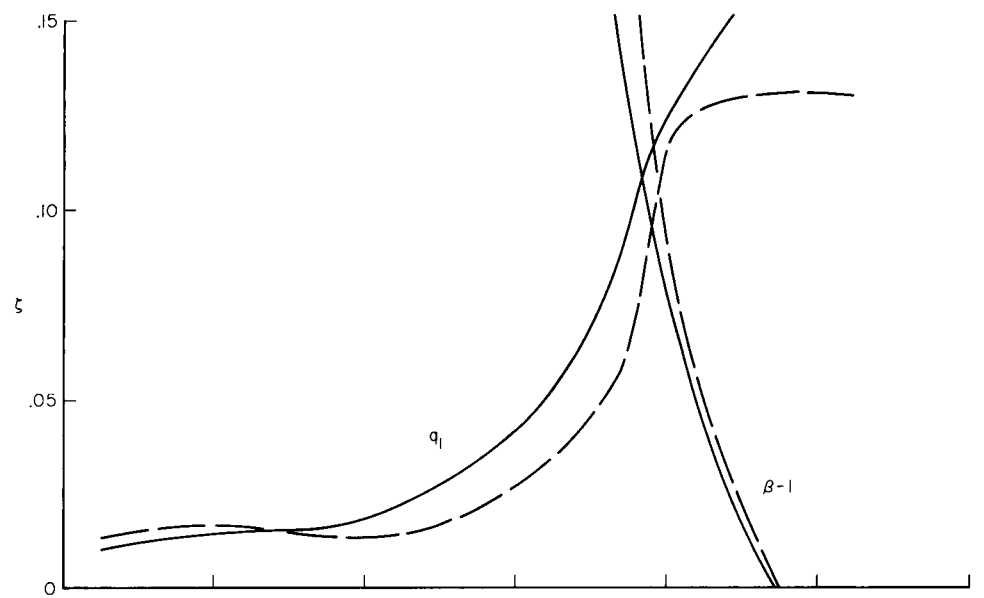


Figure 32.— Hingeless rotor: effect of using both uncoupled blade-bending modes and only  $c_{1\alpha}$  terms for rotor aerodynamics.

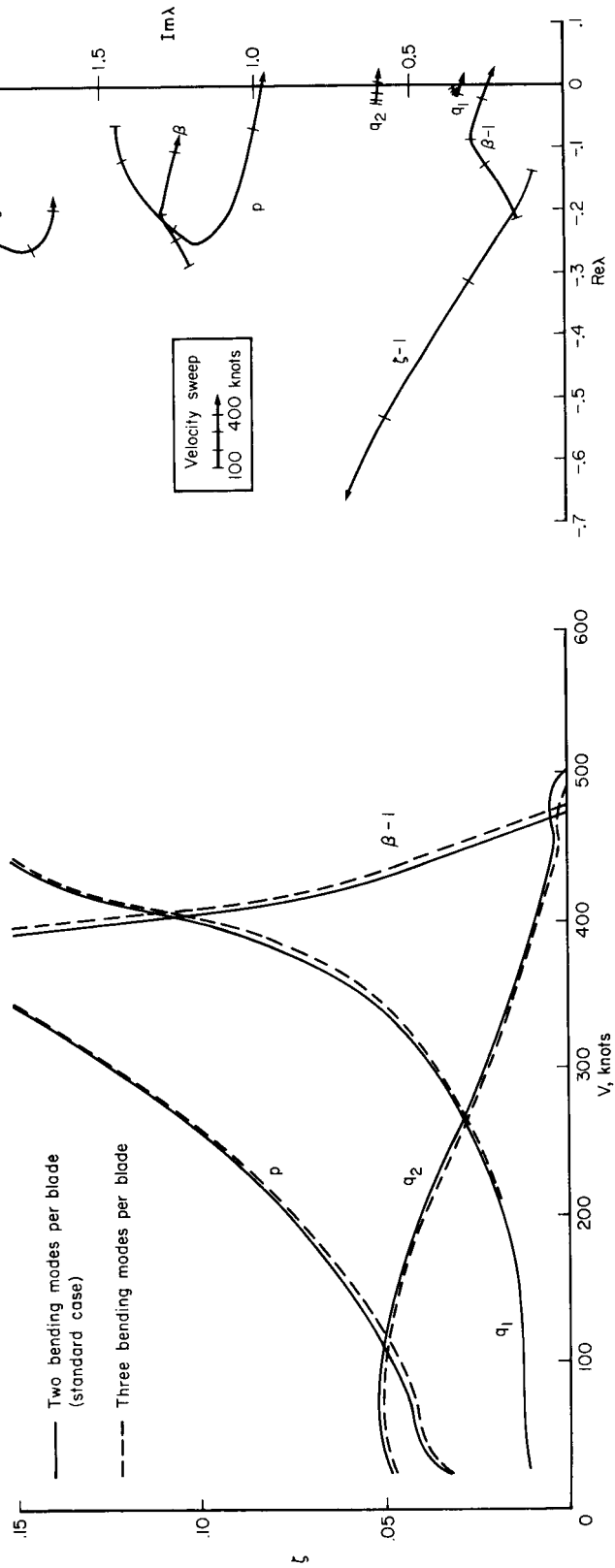


Figure 33.— Hingeless rotor: effect of using three bending modes per blade, compared with using two modes (base case).

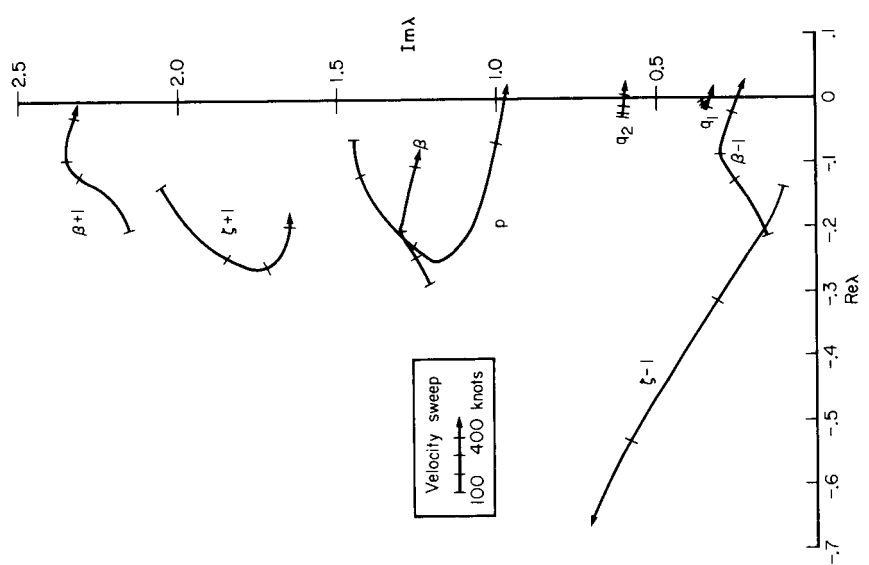


Figure 34.— Hingeless rotor: root locus for velocity sweep at  $\Omega = 386$  rpm and windmilling rotor; rotor blade pitch and torsion degrees of freedom are included.

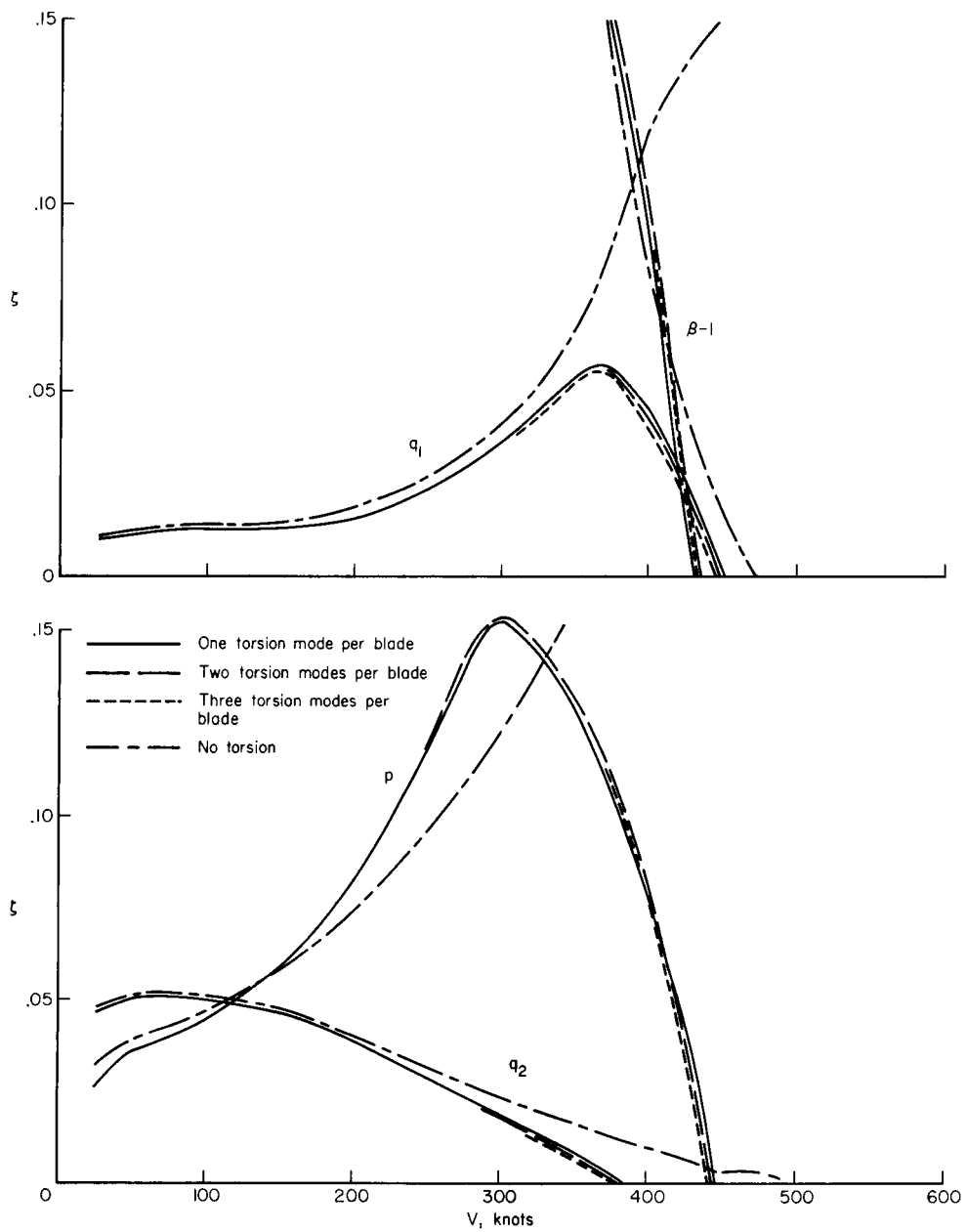


Figure 35.— Hingeless rotor: influence of rotor blade torsion dynamics, comparing the damping ratio of the wing modes using one to three, or no torsion degrees of freedom per blade.

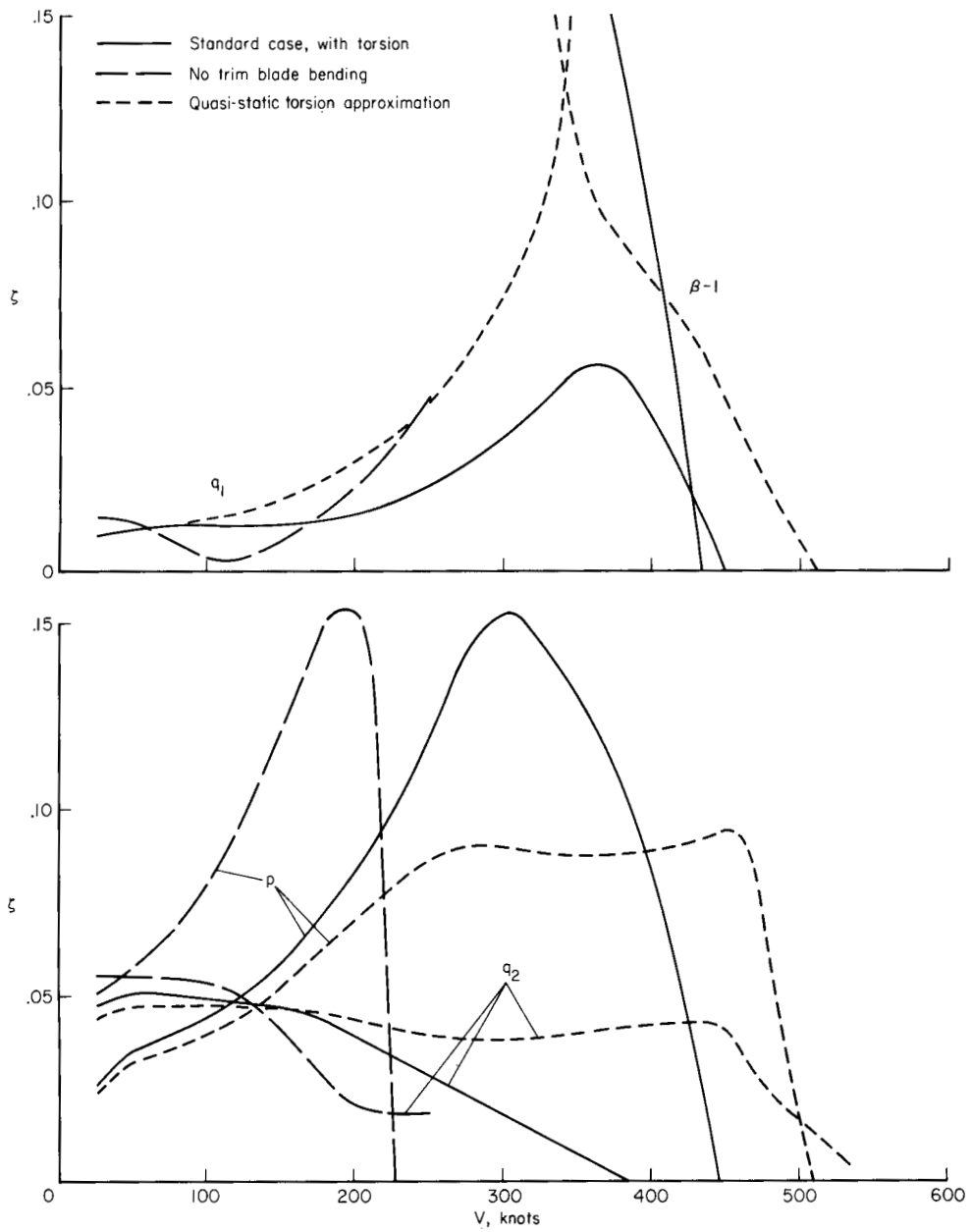


Figure 36.— Hingeless rotor: wing mode damping, showing influence of blade-trim bending deflection and of quasi-static torsion approximation when the blade torsion dynamics are involved.

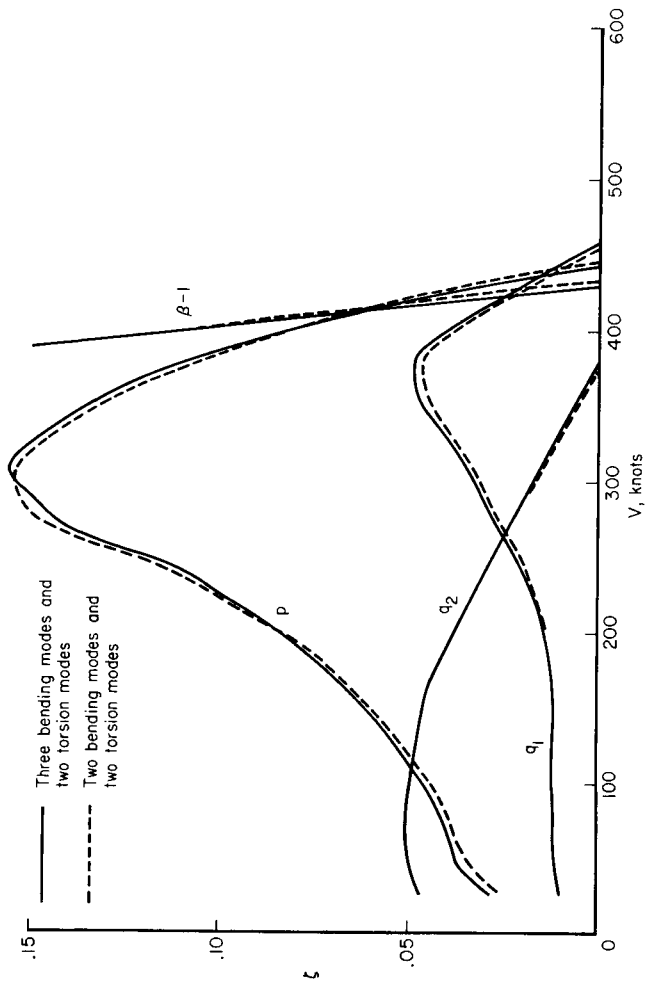


Figure 37.— Hingeless rotor: effect of using two and three blade bending modes, including blade torsion dynamics.

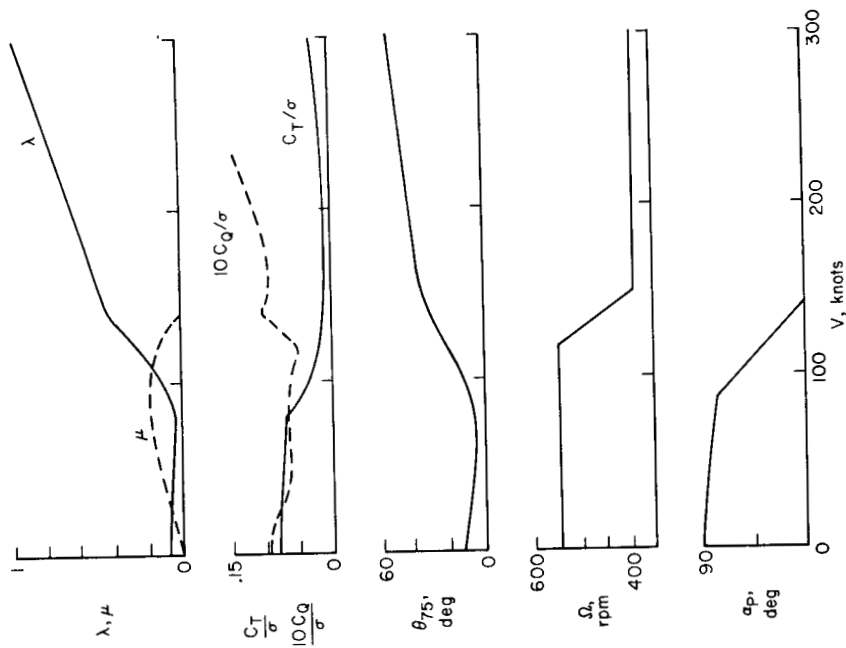


Figure 38.— Hingeless rotor: variation of parameters on flight path including conversion from helicopter to airplane mode of operation.

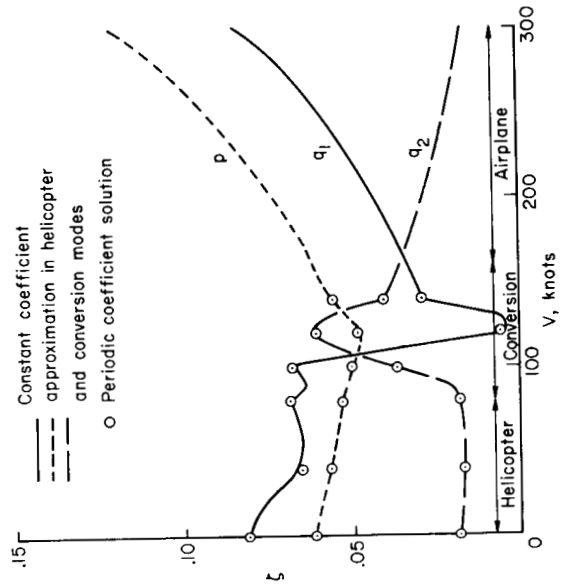
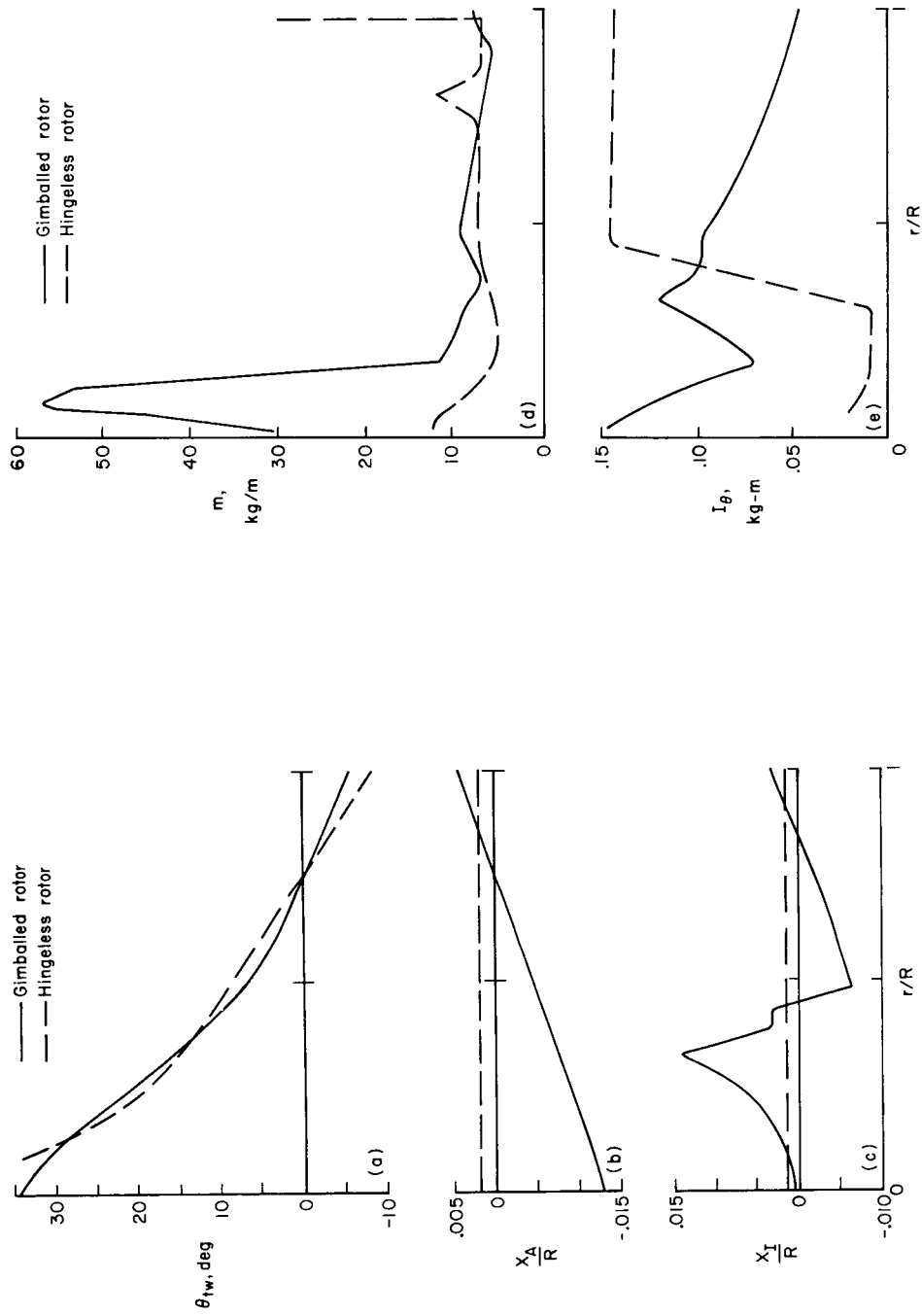
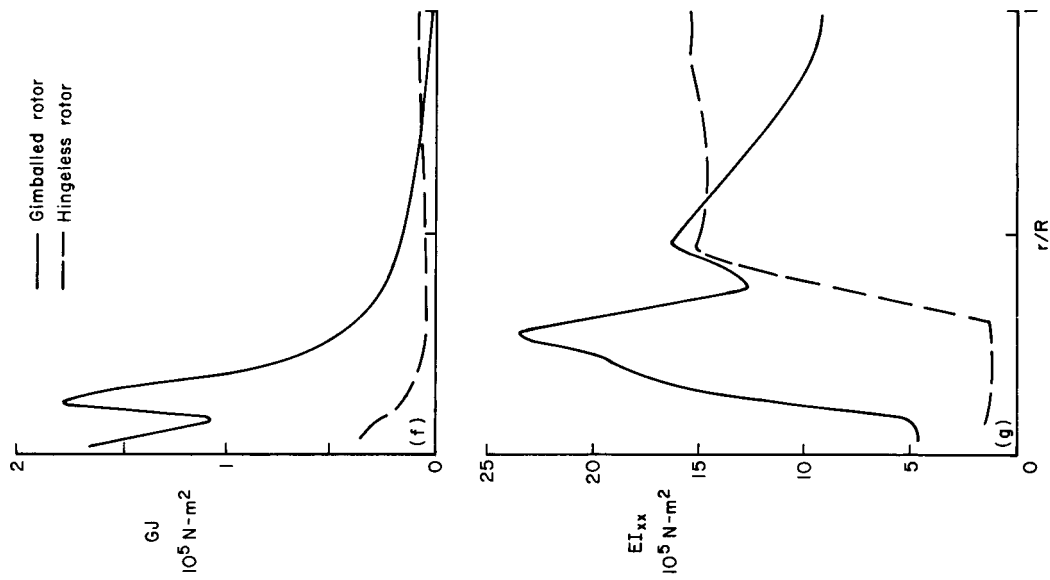


Figure 39.— Hingeless rotor: damping ratio of wing modes on flight path through conversion, comparing results of constant coefficient approximation with periodic coefficient solutions.



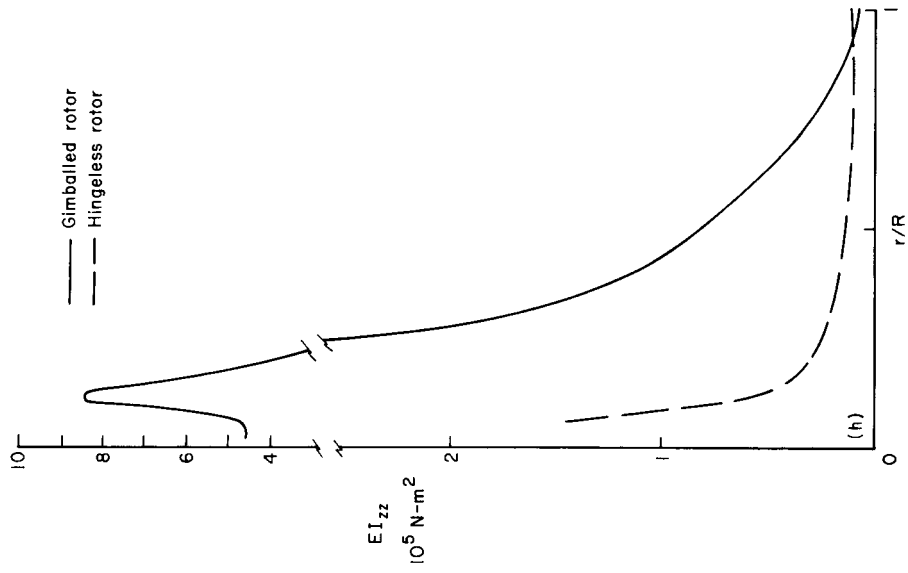
(a) Twist  
 (b) Distance aerodynamic center aft feathering axis.  
 (c) Distance center of gravity aft feathering axis.  
 (d) Section mass.  
 (e) Section torsional moment of inertia.

Figure 40.— Radial distribution of blade properties, for gimballed and hingeless rotors analyzed.



(f) Torsion stiffness.

(g) Chordwise bending stiffness.



(h) Flatwise bending stiffness.

Figure 40. — Concluded.

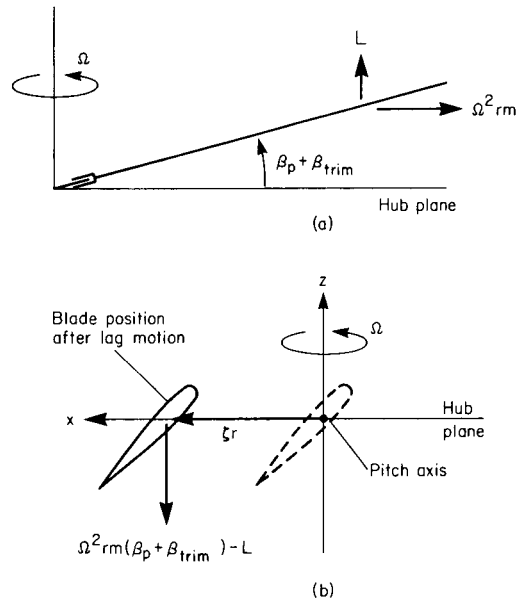


Figure 41.— Sketch of the origin of the blade pitch motion effects on propotor dynamics.

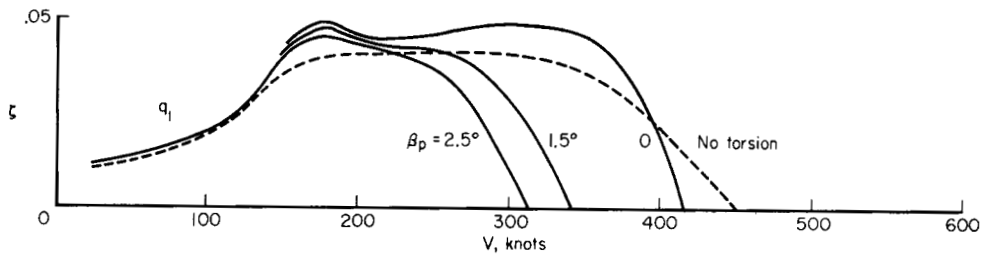


Figure 42.— Gimbaled rotor: influence of precone on effect of blade-pitch dynamics; wing vertical bending damping ratio for  $\beta_p = 2.5^\circ$  (base),  $1.5^\circ$ ,  $0^\circ$ , and no torsion result.

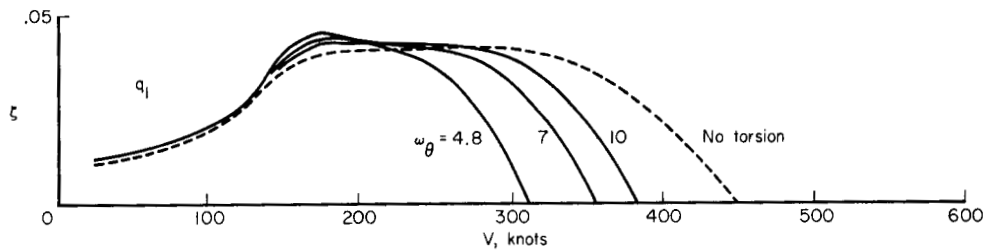


Figure 43.— Gimbaled rotor: influence of pitch natural frequency on effect of blade-pitch dynamics; wing vertical bending damping ratio for  $\omega_\theta = 4.8/\text{rev}$  (base),  $7/\text{rev}$ , and  $10/\text{rev}$ , and no torsion result.

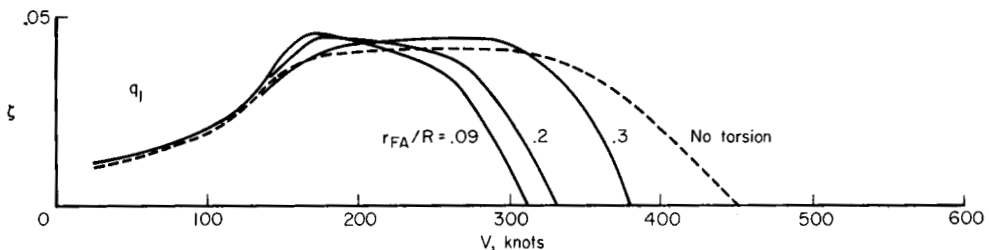


Figure 44.— Gimbaled rotor: influence of pitch bearing radial location (hence lag bending flexibility inboard of the pitch bearing) on effect of blade-pitch dynamics; wing vertical bending damping ratio for  $r_{FA}/R = 0.09$  (base),  $0.2$ , and  $0.3$ , and for no torsion result.



POSTMASTER: If Undeliverable (Section 158  
Postal Manual) Do Not Return

*"The aeronautical and space activities of the United States shall be conducted so as to contribute . . . to the expansion of human knowledge of phenomena in the atmosphere and space. The Administration shall provide for the widest practicable and appropriate dissemination of information concerning its activities and the results thereof."*

—NATIONAL AERONAUTICS AND SPACE ACT OF 1958

## NASA SCIENTIFIC AND TECHNICAL PUBLICATIONS

**TECHNICAL REPORTS:** Scientific and technical information considered important, complete, and a lasting contribution to existing knowledge.

**TECHNICAL NOTES:** Information less broad in scope but nevertheless of importance as a contribution to existing knowledge.

**TECHNICAL MEMORANDUMS:** Information receiving limited distribution because of preliminary data, security classification, or other reasons. Also includes conference proceedings with either limited or unlimited distribution.

**CONTRACTOR REPORTS:** Scientific and technical information generated under a NASA contract or grant and considered an important contribution to existing knowledge.

**TECHNICAL TRANSLATIONS:** Information published in a foreign language considered to merit NASA distribution in English.

**SPECIAL PUBLICATIONS:** Information derived from or of value to NASA activities. Publications include final reports of major projects, monographs, data compilations, handbooks, sourcebooks, and special bibliographies.

**TECHNOLOGY UTILIZATION PUBLICATIONS:** Information on technology used by NASA that may be of particular interest in commercial and other non-aerospace applications. Publications include Tech Briefs, Technology Utilization Reports and Technology Surveys.

*Details on the availability of these publications may be obtained from:*

**SCIENTIFIC AND TECHNICAL INFORMATION OFFICE**

**NATIONAL AERONAUTICS AND SPACE ADMINISTRATION**

**Washington, D.C. 20546**